Guard Your Heart Silently: Continuous Electrocardiogram Waveform Monitoring with Wrist-Worn Motion Sensor

YETONG CAO, Beijing Institute of Technology, China
FAN LI*, Beijing Institute of Technology, China
HUIJIE CHEN, Beijing University of Technology, China
XIAOCHEN LIU, Beijing Institute of Technology, China
LI ZHANG, HeFei University of Technology, China
YU WANG, Temple University, USA

In recent years, particular attention has been devoted to continuous electrocardiogram (ECG) waveform monitoring due to its numerous applications. However, existing solutions require users to be confined to particular locations, rely on dedicated and expensive hardware, or require active user participation. The constrained recording conditions prevent them from being deployed in many practical application scenarios. In view of this, we present *VibCardiogram*, a continuous and reliable design for estimating ECG waveform shape via ubiquitous wrist-worn wearables; it renders a personal ECG waveform shape estimating system with prolonged recording time accessible to a larger sector of the population. Instead of adding auxiliary sensors to wearables, *VibCardiogram* leverages the widely integrated motion sensor to characterize cardiac activities, and interpret them to generate an alternative signal that has the same waveform shape as the ECG signal. Specifically, *VibCardiogram* extracts the cardiogenic body vibrations from noisy sensor data. As the waveform variability and inconstant period hinder the segmentation of cardiac cycles, *VibCardiogram* extracts features and realizes accurate segmentation via machine learning. To parse cardiac activities from vibration signals, we build a deep-learning pipeline associating the encoder-decoder framework and Generative Adversarial Networks. With dedicated construction and training, it can estimate the ECG waveform accurately. Experiments with 20 participants show that *VibCardiogram* can achieve an average estimation error of 5.989% for waveform amplitude estimation, which is within the 10% margins regulated by the American National Standards Institute. Moreover, the promising results further confirm that *VibCardiogram* effectively extracts Heart Rate Variability features and supports downstream applications.

CCS Concepts: • **Human-centered computing → Ubiquitous and mobile computing systems and tools**.

Additional Key Words and Phrases: Wearable, cardiogenic body vibration, deep learning, ECG

ACM Reference Format:
Yetong Cao, Fan Li, Huijie Chen, Xiaochen liu, Li Zhang, and Yu Wang. 2022. Guard Your Heart Silently: Continuous Electrocardiogram Waveform Monitoring with Wrist-Worn Motion Sensor. *Proc. ACM Interact. Mob. Wearable Ubiquitous Technol.* 6, 3, Article 103 (September 2022), 29 pages. https://doi.org/10.1145/3550307

*Corresponding author.

Authors' addresses: Yetong Cao, yetongcao@bit.edu.cn, Beijing Institute of Technology, Beijing, China; Fan Li, Beijing Institute of Technology, Beijing, China, fli@bit.edu.cn; Huijie Chen, Beijing University of Technology, Beijing, China, chenhuijie@bjut.edu.cn; Xiaochen liu, Beijing Institute of Technology, Beijing, China, xiaochenliu@bit.edu.cn; Li Zhang, HeFei University of Technology, Hefei, Anhui, China, lizhang@hfut.edu.cn; Yu Wang, Temple University, Philadelphia, Pennsylvania, USA, 19122, wangyu@temple.edu.

2474-9567/2022/9-ART103 $15.00
https://doi.org/10.1145/3550307

1 INTRODUCTION

The rise of Electrocardiogram (ECG) technologies fuels the proliferation of various emerging biomedical applications, such as emotion recognition[31], biometric identification[76], and measuring personal physiological metrics[36]. The ECG signal basically corresponds to the cardiac activities and has a unique waveform shape associated with cardiac cycles. Analyzing ECG waveform shapes can provide meaningful information for characterizing heart functionality [65]. Traditionally, people can get their ECG by placing 3-12 wet Ag/AgCl electrodes on the torso with electrolyte gel [43]. However, it requires expertise thus is only performed in clinical settings. Recently, researchers have integrated sensors and electrodes into household facilities (e.g., beds [59], toilet seats [42], chairs [50], and ceiling-mounted microwave devices [85]) for ECG monitoring. Although enabling a relatively more flexible deployment setting, users are still restricted to specific locations related to these facilities, which easily causes inconvenience.

Enabling a new hands-free and less-disrupting sensing modality, wearable computing has attracted tremendous attention due to its numerous applications [12, 23, 68]. For instance, fabric electrodes have been woven or stitched directly into textiles [61], garments [37], and belts [62] for wearable ECG monitoring. However, the use of expensive dedicated hardware prevents them from being adopted widely. Alternatively, a serious push is evident on integrating electrodes into smartwatches, such as Apple Watch [4] and Galaxy Watch [3]. However, they require users to cover the electrodes with their fingers and constrained recording conditions (e.g., avoid body motions). Therefore, there still requires an alternative solution to enable continuous, convenient, unobtrusive, and reliable ECG waveform shape inferring to a larger sector of the population.

There exist many cardiac-related techniques that can monitor heart rate, blood oxygen, photoplethysmogram (PPG) signals, and even Heart Rate Variability (HRV) features via ubiquitous wearables, why do we still need a new system for inferring ECG waveform? First of all, these parameters only capture cardiac activities in abstract form and convey part of the cardiac activities, so they are not applicable to application scenarios demanding fine-grained cardiac activity information. In contrast, the waveform of ECG provides direct information about heart functions, which can support versatile applications [31, 76] and help doctors determine the cause of specific symptoms [5]. To emphasize this, Table 1 compares these parameters with ECG in the ability to monitor mental states and physiological metrics. Therefore, it is important to extract ECG waveform shapes to gain insights into fine-grained heart functions. Secondly, existing solutions for these cardiac-related signs are subject to the same "curse" of body motions, as body/arm/hand motions usually overwhelm the subtle excitation signals caused by cardiac procedures. So they mostly discard data contaminated by body motions and thus impair continuity. Motion-robust monitoring remains a relatively less-studied field, which still lacks highly effective solutions.

In this paper, we propose *VibCardiogram*, a new low-cost wearable technology that can continuously, reliably, conveniently, and unobtrusively sense heart-activity-induced vibrations from the wrist and further render a

Table 1. Comparisons of ECG with typical cardiac-related parameters in monitoring mental states and physiological metrics.

Parameter	Work	Fatigue	Stress	Heart Age	HAC	CHD	CeVD	RHD	EHB
Heart Rate	[70]	×	×	×	✓	×	×	×	×
HRV	[17, 63, 67]	✓	✓	✓	✓	×	×	×	×
Blood oxygen	[33]	✓	✓	×	×	×	×	×	×
PPG	[14, 46]	✓	✓	✓	✓	×	×	×	×
ECG	[19, 69, 79]	✓	✓	✓	✓	✓	✓	✓	✓

HAC: heart arrhythmia conditions; CHD: coronary heart disease; CeVD: cerebrovascular disease; RHD: rheumatic heart disease; EHB: ectopic heart beat.

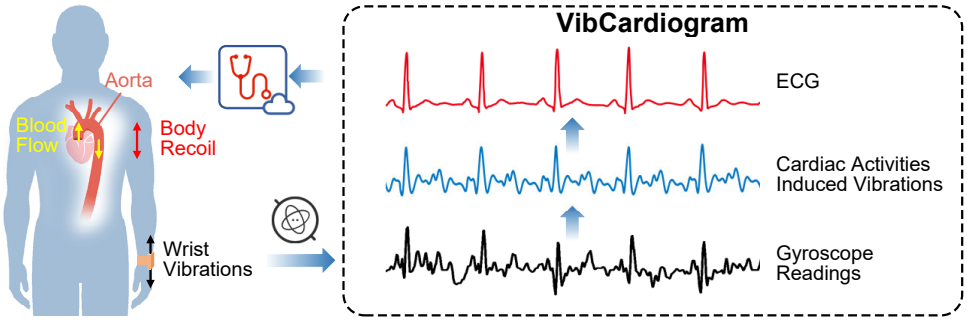

Fig. 1. The concept of *VibCardiogram*.

personal ECG waveform shape estimating system with prolonged recording time accessible to a larger sector of the population. We envision *VibCardiogram* as a vital solution for mobile health sensing by transforming ubiquitous smartwatches into biosensing devices. The basic idea is inspired by our finding that the Inertial Measurement Unit (IMU) of wrist-worn devices can sense the subtle body vibration induced by cardiac activities during the heart beating process, which has been widely validated in clinical practice [27, 32]. Fig. 1 shows the concept of *VibCardiogram*. The mass center of blood shifts periodically in response to the ejection of blood into the aorta caused by cardiac activities (i.e., systole and diastole); this induces body vibrations associated with recoil forces, and reaches the wrist-worn deceive via surface propagation. From prior work [59], we know that ECG signals have unique waveform shapes corresponding to heart activities in the cardiac cycle. Through novel construction, *VibCardiogram* extracts the cardiogenic body vibrations from noisy sensor data and learns the mapping between cardiogenic body vibration patterns and the simultaneous ECG waveform shapes.

Despite the simple idea, three major challenges underlie the design: (1) **How to effectively disentangle the wrist vibration induced by cardiac activities from noisy sensor data collected at the wrist?** Wrist-worn devices are usually associated with body motion from daily activities (e.g., walking and cooking), which usually significantly affect the sensing quality. To realize motion-robustness sensing, we carefully study the characteristic of cardiogenic body vibrations under various motion scenarios; this motivates us to profile motion interference by time-frequency analysis. Particularly, we propose a novel Stationary Wavelet Transform (SWT)-based method to extract cardiogenic body vibrations. Moreover, we leverage the normalized Least Mean Square (LMS) algorithm with variable step-size adjustment to accommodate noise level differences. (2) **How to effectively segment each heartbeat in the complex cardiogenic body vibrations?** Fine-grained ECG waveform shape estimation requires profiling the detailed cardiac activities by performing accurate heartbeat segmentation. However, the time-varying waveform and inconstant period of cardiogenic body vibrations (result from the dynamic nature of the heartbeat) make it very challenging. Through studying the characteristics of sensor data, we extract four features from the vibration waveform, which captures the unique geometric pattern of beat boundaries. Given the features, we perform heartbeat segmentation leveraging the power of machine learning. (3) **How to achieve accurate and fine-grained ECG waveform shape estimation?** *VibCardiogram* infers ECG waveform shapes by profiling detailed cardiac activities in the extracted vibration segments. However, the relationship between ECG waveform and vibration waveform collected from the wrist is unclear and rarely studied, making ECG waveform shape inferring very difficult. Moreover, reconstruction of the ECG waveform shape requires the system to gain a comprehensive understanding of cardiac activities through wrist vibrations. However, only partial knowledge can be obtained using a single wearable mobile device, which usually integrates only one motion sensor. To address these, we equip *VibCardiogram* with a deep-learning pipeline associating the encoder-decoder framework and Generative Adversarial Networks (GAN). With dedicated construction and training, it can convert the cardiogenic body vibrations into ECG measurements. Our main contributions are summarized as follows:

(1) We demonstrate that low-cost motion sensors integrated into wrist-worn devices can be utilized to reconstruct ECG waveform shapes. To the best of our knowledge, *VibCardiogram* is the first system based on the low-cost motion sensor on a wrist-worn device that empowers users for continuous, reliable, convenient, and unobtrusive ECG waveform shape estimating. The idea potentially reshapes the daily experience of mobile biosensing, which could greatly advance biomedical applications.
(2) We propose several novel algorithms that can effectively remove body movement interference and segment wrist vibration in each heartbeat cycle. Besides, we design a novel deep learning pipeline, leveraging the benefits of the encoder-decoder technique and GAN, to reconstruct ECG waveform shapes based on wrist vibrations.
(3) We implement *VibCardiogram* and conduct extensive experiments with 20 participants. The average estimation error is 5.989%, which is within the acceptable range regulated by the American National Standards Institute ($\leq$ 10%). Besides, the average correlation coefficient is 0.926, which validates the effectiveness of *VibCaridogram* for estimating ECG waveform shapes. Moreover, we showcase an application of emotion recognition based on *VibCardiogram*, demonstrating its capabilities in supporting biosensing development.

The rest of this paper is organized as follows: Section 2 introduces the preliminaries. Section 3 presents the overview of *VibCardiogram* and elaborates on the detailed system designs. Section 4 evaluates the performance of *VibCardiogram*. In Section 5, we review the related works, followed by discussion and further work in Section 6. Finally, we conclude the paper in Section 7.

2 PRELIMINARIES

In this section, we first introduce the generation mechanisms of ECG signals and cardiogenic body vibrations, respectively. Because ECG signals and cardiogenic body vibrations characterize the same cardiac activities from different dimensions, they can be temporally correlated to offer interconversion, like translating a phrase from one language to another. Then, we study the feasibility of capturing the cardiogenic body vibrations using the IMU sensor on wrist-worn devices, which provides the basics of *VibCardiogram*.

2.1 ECG Waveform Shape and Cardiac Activities

An ECG signal measures the electrical activity generated by the heart muscle. ECG from a healthy human has a unique waveform shape, as shown in Fig. 2, which includes P wave, QRS complex, and T wave. QRS complex indicates ventricular depolarization, causing ventricles contraction, ejecting blood out of the ventricles rapidly, and marks the beginning of systole. As ventricular repolarization, indicated by the T wave, the blood flows through the body into the atria and then fills ventricles passively, which marks the end of systole and beginning of diastole. And the P wave indicates atrial depolarization, resulting in simultaneous contraction of the atria, and forcing blood into the ventricles. Any irregular cardiac rhythm and heart block would change the cardiac

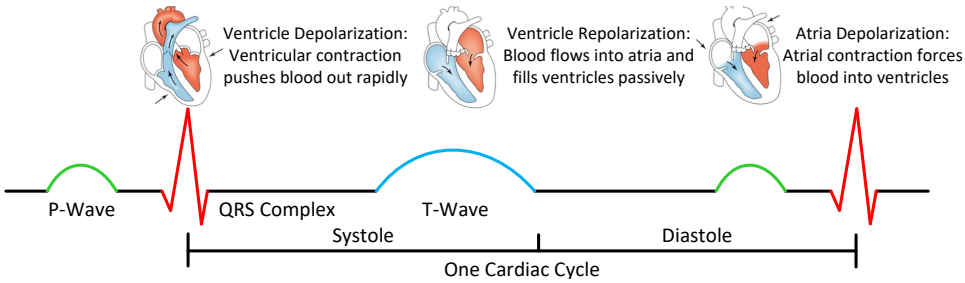

Fig. 2. An example of common waveform of an ECG signal with the associated cardiac activities.

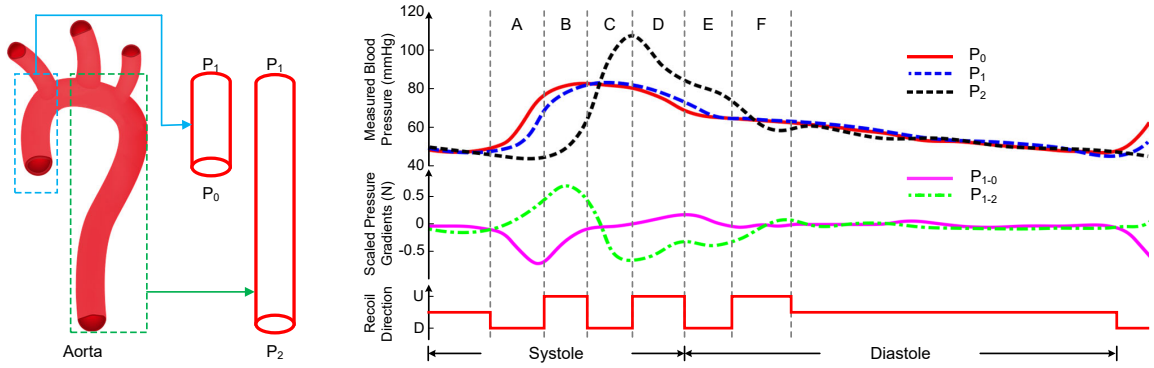

(a) The aorta and its simplified model

(b) An example of blood pressure and scaled pressure gradients. U and D represent upward and downward, respectively

Fig. 3. Mechanism for the genesis of cardiogenic body vibration [38].

activities, thereby distorting the ECG waveform shape. Physicians have directed attention to the analysis of ECG waveform shapes for spotting cardiac complications, especially towards potential complications of COVID-19 ranging from arrhythmia to acute cardiac injury [9, 20].

2.2 Cardiogenic Body Vibrations and Cardiac Activities

The body vibrations that accompany cardiac activities have long been widely observed [11, 35, 59]. The principal mechanism for the genesis of cardiogenic body vibration is Newton's third law of motion; namely, there is a reacting force of equal magnitude and the opposite direction for every acting force. As the mass of the circulating blood moves during periods of cardiac systole and diastole, the body recoils periodically and causes repeated vibrations to the human body.

Herein, we reveal the detailed mechanism by the blood pressie gradients in the ascending and descending aorta. As shown in Fig. 3(a), the aorta is usually simplified as two tubes in cascade, representing the ascending and descending aorta, respectively. Fig. 3(b) shows an example of blood pressure measured from different locations, the scaled pressure gradients, and the body recoil directions. P_0, P_1, and P_2 denote the blood pressure of the aorta inlet, the apex of the aortic arch, and the aorta outlet. Moreover, $P_{1-0} = P_1 - P_0$ represents the pressure gradients between P_1 and P_0, and $P_{1-2} = P_1 - P_2$ represents the pressure gradients between P_1 and P_2, respectively. There are basically six phases characterizing different body vibrations in response to cardiac systole and diastole: (i) At the beginning of systole, ventricular contraction (QRS complex in ECG signal) forces the blood into the aorta inlet. P_0 starts to increase while P_1 remains unchanged, thereby P_{1-0} decreases. The body recoils downward in response to the blood mass moving upward. (ii) Then, P_1 increases and P_2 remains unchanged, which increases P_{1-2} and increases the blood volume rapidly between the apex of the aortic arch and aorta outlet, leading to the body recoil forces being abruptly reversed. (iii): As P_2 builds up, P_{1-2} decreases, and the blood flow decelerates, which is equivalent to applying an upward force. Meanwhile, a downward recoil of the body occurs. (iv): Right after P_2 reaches maximal, it rapidly decreases, resulting in an increase in $P_1 - 2$. Such an increase causes an upward recoil of the body. (v): In the diastole phase, relaxation of ventricles follows ventricle repolarization (T wave in ECG). P_{1-0} decreases to zero while P_{1-2} decreases to a local minimum. The blood encounters an upward reflected wave and generates a downward force on the body. (vi) Finally, the blood further moves towards the peripheral vessels and causes a decrease in P_2, creating the upward reconciliation of the body.

Based on the above, the cardiogenic body vibrations and ECG signals each characterize the cardiac activities from different dimensions. Although forming a direct one-to-one mapping is difficult, there still offers precise

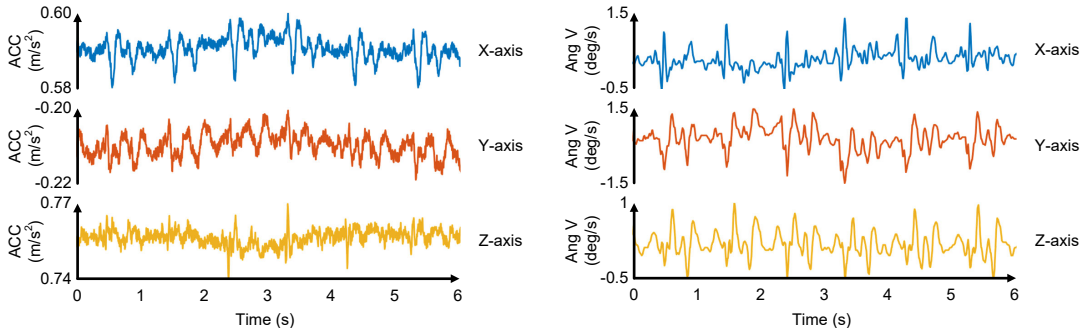

(a) Acceleormeter readings (b) Gyroscope readings

Fig. 4. An example of sensor readings of accelerometer and gyroscope.

temporally-correlation between them, which has been supported by existing studies [11, 35, 59]. Therefore we are motivated to profile the cardiogenic body vibrations as an alternative to the true ECG for supporting biosensing applications. With the number of different options available for profiling cardiogenic body vibrations, we utilize the motion sensor mounted on wrist-worn devices. Note that the recoil force of the body not only happens in the longitudinal axis of the body. Prior imaging studies [75] have shown that blood flow has a right-hand helical pattern around the ascending aorta and aortic arch at the beginning of systole. In other words, the human body produces complex recoil forces in many directions. We then study the feasibility of capturing cardiogenic body vibrations using IMU mounted on wrist-worn devices.

2.3 Capturing Cardiogenic Body Vibrations Using IMU Mounted on Wrist-Worn Devices

A commercial smartwatch is typically equipped with an IMU that contains a three-axis accelerometer and a three-axis gyroscope. We now explore the opportunity of capturing cardiac activities using readings of certain sensing modalities of IMU, and how we envisage employing it for estimating ECG waveform.

For more than a century, researchers have long investigated capturing cardiogenic body vibrations using various sensing modalities. In particular, ballistocardiography [26] (BCG) is a widely used term: It measures the reaction (displacement, velocity, or acceleration) of the whole body resulting from cardiac activities. In our initial investigation of capturing cardiogenic body vibrations using IMU sensors mounted on wrist-worn devices, we try to mimic the BCG monitoring procedure, which analyzes the accelerometer readings (Note that the BCG signal has a very different waveform shape than our reconstructed signal and the ECG signal). However, we find such measurements have a low signal-to-noise ratio (SNR) and are always affected by gravity distortion during everyday life [32] (shown in Fig. 4(a)). This makes the accelerometer readings not applicable in practice.

Prior study [57] has found that most energy transferred by the heart to the body corresponds to rotational energy (e.g., a percentage that can be as high as 95% in healthy young adults). Therefore, we use the gyroscope readings collected from the wrist (shown in Fig. 4(b)), which has been identified to be more sensitive to cardiogenic body vibrations than the accelerometer. However, another question arises: *How do we reliably capture cardiogenic body vibrations when the X, Y, and Z-axis readings of the gyroscope show different trajectories?*

To investigate this problem, we ask a volunteer to record wrist gyroscope readings. Meanwhile, we record the volunteer's ECG and phonocardiogram (PCG) signals to provide reference to cardiac activities. Fig. 5 shows an example of the captured ECG signals, PCG signals, and gyroscope signals, where G_x, G_y, and G_z are the data gathered by gyroscope along the X, Y, and Z-axis, respectively. The ECG signal characterizes the cardiac activities of systole and diastole with a P wave, a QRS complex, and a T wave. Meanwhile, the PCG signal tracks the two sounds, S_1 and S_2, of valves closure associated with the beginning of systole and diastole. We

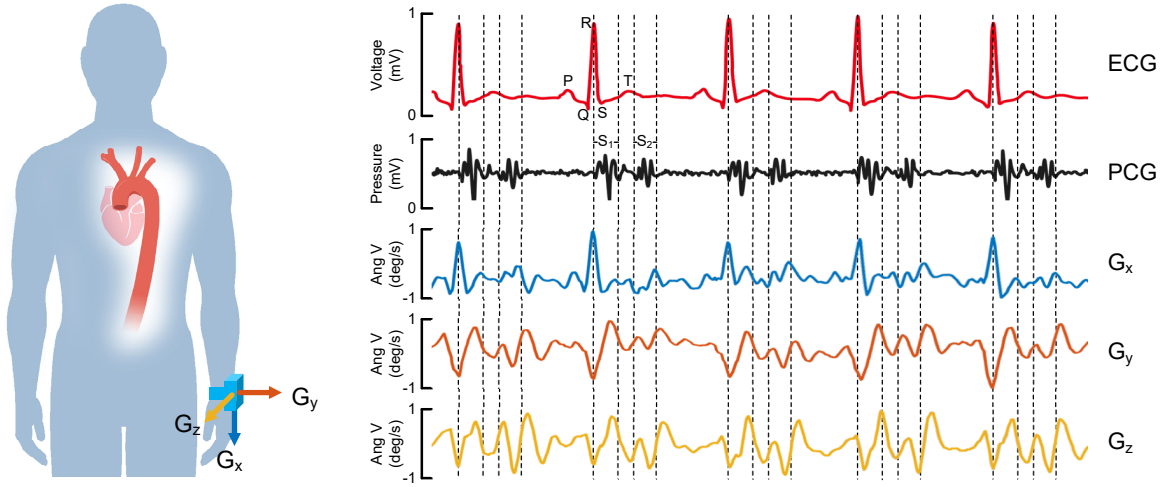

(a) Placement of the IMU and the measurement axes

(b) ECG, PCG, and wrist gyroscope readings in three orthogonal axes. Since the sampling rate is 100 Hz, there is no observable delay between body vibration and ECG since the actual time delay is less than a few tens of milliseconds.

Fig. 5. An example of the relativeing timing of ECG, PCG, and wrist gyroscope readings

can observe that G_x, G_y, and G_z all show clearly periodic heartbeat patterns. By relating ECG and PCG with them, we find that G_x experiences peak, trough, or turning points at the transition of cardiac activities. This confirms our previous conclusion that ECG and cardiogenic body vibrations are intrinsically-correlated, therefore creating an opportunity to interpret the cardiogenic body vibrations to estimate the waveform patterns of ECG signals. Through repeated experiments and validation, we identify that data from the axis in the same direction as the forearm (i.e., G_x) successfully capture the cardiac activities in various arm positions, thus is adopted by *VibCardiogram*. More encouragingly, we can observe that G_x is temporally correlated with ECG signals, which provides our design basics.

3 SYSTEM DESIGN

3.1 Overview

We propose *VibCardiogram* to complement the lack of a continuous, reliable, convenient, and unobtrusive support for ECG waveform shape estimation. Specifically, *VibCardiogram* captures the cardiogenic body vibrations using the IMU mounded on the wrist-worn device, then characterizes them and estimates ECG waveform shapes. The architecture of *VibCardiogram* is shown in Fig. 6, which can be divided into *Wrist Vibration Extraction*, *Vibration Signal Segmentation*, and *ECG Estimation*. *VibCardiogram* first takes the motion sensor readings from the wrist-worn device as input. Then, *Wrist Vibration Extraction* is conducted to remove the interference related

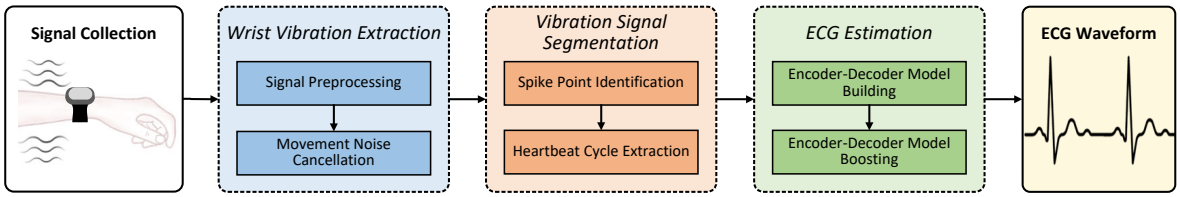

Fig. 6. System architecture of *VibCardiogram*.

to the body movement. Specifically, it obtains the vibration signals induced by cardiac activities leveraging Stationary Wavelet Transform (SWT) and normalized Least Mean Square (LMS) adaptive filtering. After that, in *Vibration Signal Segmentation*, geometric features are extracted from the clean vibration signals and classified by the machine learning technique, which allows us to identify beat boundaries and segment cardiac cycles. At last, in *ECG Estimation*, we design a deep-learning pipeline associating the encoder-decoder framework and GAN to generate accurate ECG measurements.

3.2 Wrist Vibration Extraction

3.2.1 Signal Preprocessing. Cardiac activities mostly generate signals in 5-30 Hz range [59]. According to the Nyquist sampling theorem, we set the sampling frequency to 100 Hz to allow motion sensors to accurately capture frequency components below 50 Hz. However, most available products are not guaranteed a fixed sampling frequency of the gyroscope's reading due to multiple interruptions related to high-priority tasks associated with the main CPU. To resolve the unstable sampling, we use linear interpolation to upsample the gyroscope data to a fixed sampling rate of 100 Hz. Then, we filter the data by a fourth-order Butterworth filter to eliminate frequency components out of 5-30 Hz. Since the respiratory frequency band is around 0.2-0.4 Hz [8], the body movement components generated by breathing can be removed. Afterward, we extract G_x from the filtered gyroscope data and then perform *Movement Noise Cancellation*.

3.2.2 Movement Noise Cancellation. The motion sensor in the wrist-worn wearables is particularly susceptible to body movements of daily activities, resulting in interference for ECG estimation. And such interference usually has an intensity greater than that of the signals caused by cardiogenic body vibrations. Fig. 7 shows an example of G_x recorded in the resting condition avoiding body motions and in the presence of arm motions. The top two panels show the raw data of two conditions, and the bottom two panels show the spectrum accordingly. We can observe that the arm motions introduce significant interference overwhelming the subtle cardiogenic body vibrations in both the time domain and frequency domain. Thus, removing the interference of body movement is vital and challenging for accurate cardiogenic body vibrations extraction.

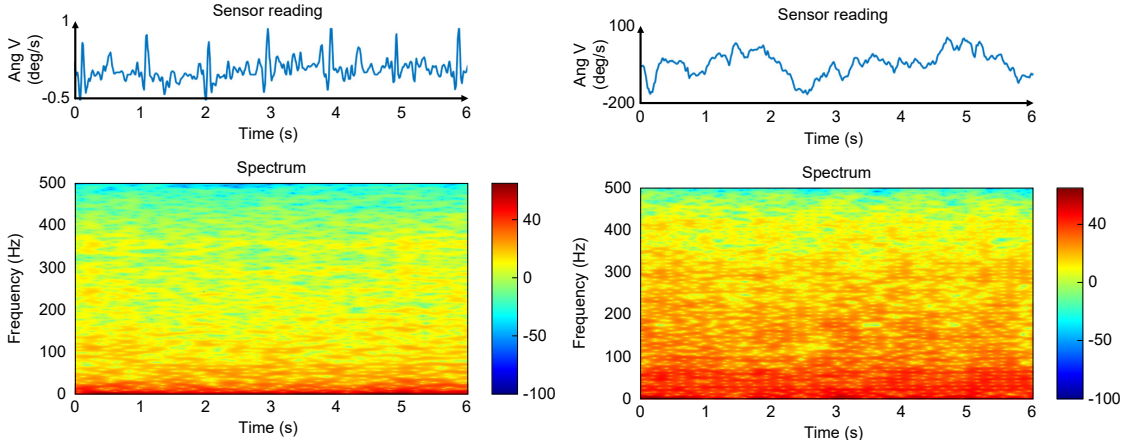

(a) Resting condition (b) Arm motion condition

Fig. 7. Comparison of G_x under resting and free motion conditions.

Intuition: Removing the movement noise from physiological signals (e.g., PPG and ECG signals) has been extensively investigated. One of the commonly used methods is to reconstruct the signal with a standard template.

However, this method is not applicable for *VibCardiogram* due to the diverse waveform patterns of wrist vibrations. Besides, principal component analysis (PCA) and independent component analysis (ICA) have been used for movement noise cancellation [15]. However, these methods will lead to artificial artifacts due to the offset of noise location in the recorded signals [49]. Alternatively, recent studies have shown the initial success of using an adaptive filter to remove the movement noise [13] The adaptive filter can self-adjust the filter coefficients in response to the distribution and characteristics of the signal. However, the adaptive filter-based approaches require additional sensors to obtain an accurate reference signal about the movement noise as an additional input. Therefore, a new challenge arises: *how to generate a reliable movement noise reference signal using a single sensing modality on the wrist?*

Inspired by Stationary Wavelet Transform (SWT) [58], which is invariant against shifts of the signal in the time domain, we design a novel method to facilitate the extraction of clean cardiogenic body vibrations. Specifically, we use the diversity of the coefficient sequences obtained by SWT to estimate movement noise reference. Then, the noise reference is input to an adaptive filter to remove the movement noise from the vibration signals.

SWT-Based Noise Reference Generation. The pipeline of the proposed SWT-based noise reference extraction method is divided into four steps:

Step 1: We first perform SWT. We implement SWT by upsampling the filter coefficients of the high pass filters and the low pass filters. In this way, we obtain a approximation coefficients sequences $\{a_1, a_2, ..., a_J\}$ and a detail coefficients sequences $\{d_1, d_2, ..., d_J\}$, where J denotes the order of SWT. Since wrist vibration signal has a frequency bandwidth of 5-30 Hz, we set J to be 6 [47]. Besides, we use the $bd4$ as the mother wavelet because it has a similar waveform shape to the wrist vibration signal. Fig. 8(b) shows the detail coefficients sequences $\{d_1, d_2, d_3, d_4, d_5, d_6\}$ of the signal in Fig. 8(a). We notice that the detail coefficients clearly demonstrate observable periodicity corresponding to cardiac cycles.

Step 2: We identify the presence of movement noise in each detail coefficient by finding parts whose magnitude reaches a significantly higher level than that of the signal caused by cardiogenic body vibrations. We first calculate the short-time energy $e_j(t)$ of the detail coefficient d_j, then detect all the local maximum amplitude $P_j(k)$ of $e_j(t)$, where $k = 1, 2, ..., K$ marks when local maximum occur. After that, we calculate the mean $\hat{\mu_j}$ and scale $\hat{\sigma_j}$ of $P_j(k)$. Specifically, we use the median and the normalized median absolute deviation to robustly estimate the two factors. Then, we determine the upper threshold of $e_j(t)$, which is calculated based on the empirical rule [44]:

$$T_j^{up} = \hat{\mu_j} + 3\hat{\sigma_j}. \tag{1}$$

If the $P_j(k)$ falls below the upper threshold, it is identified as the wrist vibration induced by cardiac activities.

Step 3: Furthermore, we consider a scenario where the amplitude level of movement noise is similar to the wrist vibration signal, supplementing the step 2. We identify such movement noise based on the fact that peaks/troughs associated with cardiac activities appear periodically, while those associated with movement noise do not. Specifically, we track the time interval between adjacent local maximums $P_j(k-1)$ and $P_j(k)$, and denote the interval as $T_j(k)$. The interval threshold $T_{interval}$ is calculated as the median value of $T_j(k)$, which is determined through experiments. If $T_j(k)$ and $T_j(k+1)$ exceed $T_{interval}$, $P_j(k)$ is identified as cardiac activities-originated.

Step 4: We separate the movement noise and signals caused by cardiogenic body vibrations and generate a continuous movement noise sequence instead of few points to input to the adaptive filter. After locating those local maximums $P_j(k)$ caused by cardiac activities, we further search forward and backward to locate the starting and ending points of $P_j(k)$. Therefore, we track the time segments that correspond to cardiac activities. Then, we replace these segments in the original detail coefficients to zero. After that, by inverse SWT, we generate the movement noise reference, as shown in Fig. 8(c). The reference not only captures the additive movement noise but also tracks very subtle constant noise in the system.

Adaptive Filter-Based Noise Cancellation. Considering that movement noise level varies during the day, we use a normalized LMS algorithm with variable step-size adjustment [39]. The step size is adjusted to be large

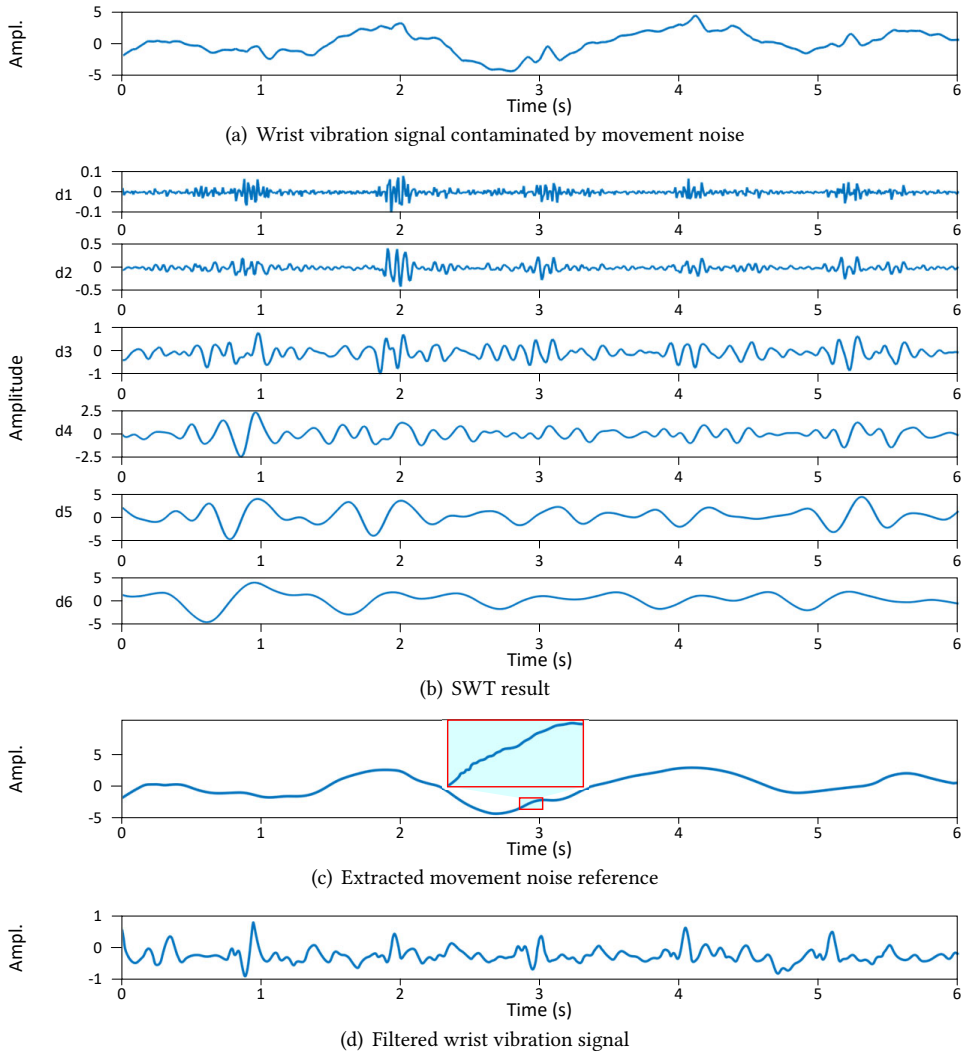

(a) Wrist vibration signal contaminated by movement noise

(b) SWT result

(c) Extracted movement noise reference

(d) Filtered wrist vibration signal

Fig. 8. An example of movement noise cancellation.

at high SNR and small at low SNR, thereby achieving robustness in real-life environments. The step size adaptive function $f(n)$ is proportional to the change of the movement noise reference signal $N(n)$ and the input wrist vibration signal $WV(n)$, defined as follows,

$$c(n) = \sigma_{N(n)} \cdot \sigma_{WV(n)}/p$$
$$f(n) = \begin{cases} f_0, & 0 \leqslant c(n) < f_0 \\ c(n), & f_0 \leqslant c(n) < 0.9 \\ 0.9, & 0.9 \leqslant c(n) \end{cases}, \tag{2}$$

where σ is the standard deviation of the signal during the last half cycle of the heart rate. The heart rate does not need to be strictly accurate and we determine it by the autocorrelation method [7]. f_0 and p are the experimentally

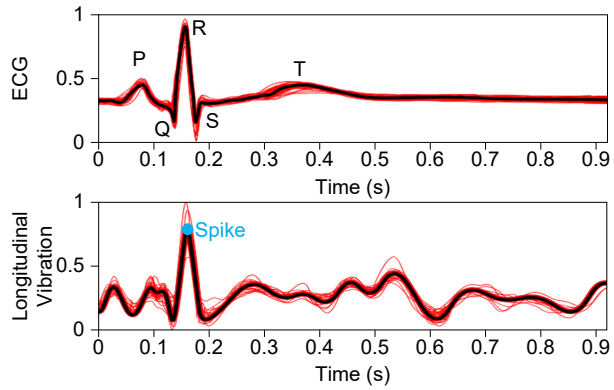

Fig. 9. Examples of ensemble average of ECG and longitudinal vibration (i.e., G_x).

determined constant, which set the $f(n)$ between 0 and 1. The step size is kept at a very small value with small movement noise during the resting period. As the noise on the wrist vibration signal increases, the step size increases. Such a scheme can trace the high frequency or non-stationary movement noise with fast speed while preventing distortion in the input signals. Fig. 8(d) shows the final output of cardiogenic body vibrations, which is calculated based on the original signal (Fig. 8(a)) and the movement noise reference (Fig. 8(c)). We can observe that the characteristics of repeated cardiac activities are reserved. Subsequently, the output wrist vibration signal range is scaled to the bound $[-1, 1]$. Experiments with various wrist movements suggest that the proposed algorithm is effective. Experiment details are presented in Section 4.3.

3.3 Vibration Signal Segmentation

Due to the dynamic nature of cardiac activities (e.g., the time interval between consecutive heartbeats always varies), cardiogenic body vibrations can have variable waveform shapes. Moreover, the compliance of the body structure imposes some modification on the cardiogenic body vibrations collected from the wrist. Fig. 8(d) shows an example of vibration data extracted by *Wrist Vibration Extraction*. Although showing potential periodicity, it is still very difficult to determine each heartbeat's boundaries since it lacks clear features. After multiple attempts, neither the autocorrelation method [60] nor the frequency method [54] failed to accurately segment each heartbeat in the vibration signals. Therefore, we propose to leverage the great power of machine learning.

Fig. 9 shows the ensembled averages (black) of the raw signals (red) that temporally aligned over 50 beats. We find that the ensembled average shows a significant upward or spike (denoted as S point) with respect to the

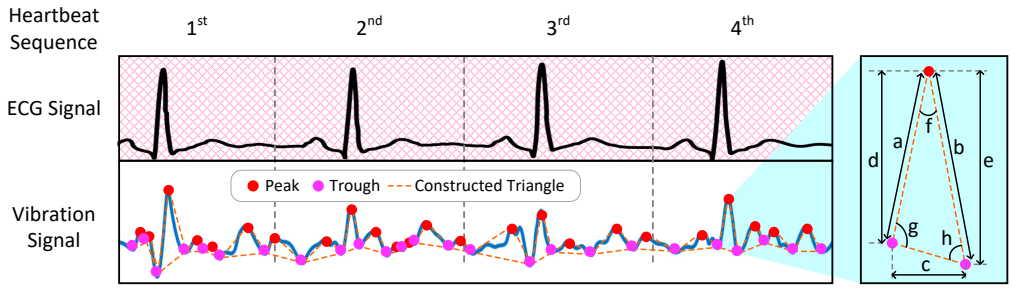

Fig. 10. An illustration of the strategy for extracting features from the wrist vibration signal.

reference ECG R peak; this could facilitate the segmentation. In particular, we use the term "spike point" to refer to the *S* point.

3.3.1 Spike Point Identification. Spike point is a special sharp local maximum point. We extract several geometric features as representatives of the shape of each local maximum point. As shown in Fig. 10, we first detect all local maximum/minimum points in the vibration sequence. Then, a triangle model is constructed for each local maximum point (peak) combined with its two adjacent local minimum points (trough). For each triangle, we identify eight parameters, as shown in the right panel Fig. 10. Our experiment with 20 volunteers finds that seven geometric features (shown in Table 2) can provide wonderful discriminating capability between actual spike points and other local maximum points. Particularly, Fig. 11 shows the t-SNE projection of the seven geometric features of all 20 subjects; this clearly demonstrates observable distinctions.

However, training a classier using them directly led to low accuracy since there is a correlation between these features. Thus, we detect the correlation between these geometric features by comparing the parameter of the Variance Inflation Factor (VIF). Overall, we select four features, including *a+b*, *d*, *e*, and *f* for training. With these selected features, we also study the performance of seven highly used classifiers, including random forest, support vector machine, least squares support vector machine, k-nearest neighbors, decision trees, logistic regression, and Naive Bayes. The detailed results are presented in Section 4.3, which shows that the random forest classifier achieves the best performance of 96.6% balanced accuracy. Thus, random forest is adopted by *VibCardiogram*.

3.3.2 Heartbeat Fragment Extraction. After finding the spikes, we need to further locate the boundaries of the heartbeat. It is desirable to obtain the wrist vibration segments that contain a whole cardiac cycle (i.e., it contains both systole and diastole phases). Based on our observation that the spike point and ECG R peak (sharp systole) are temporally relevant, we adopt the segmentation technique from the ECG field. We identify the 250 ms before the spike point as the onset of a heart cycle; this is widely adopted for heartbeat region segmentation for ECG signals [88]. Meanwhile, such onset is regarded as the endpoint of the previous segment to cover a whole heartbeat cycle.

Table 2. Comparison of geometric features between spike points and other points.

Feature	Spike points			Other points		
	AVG	MED	STD	AVG	MED	STD
a+b	1.221	1.165	0.384	0.427	0.349	0.104
c	0.160	0.150	0.004	0.093	0.08	0.004
d	0.470	0.433	0.009	0.221	0.150	0.046
e	0.738	0.803	0.238	0.189	0.094	0.061
f	0.385	0.324	0.043	0.848	0.698	0.295
g	0.971	0.491	0.954	1.253	1.364	0.815
h	1.355	0.840	1.064	1.041	0.574	0.985

AVG stands for average; MED stands for median; STD stands for standard deviation.

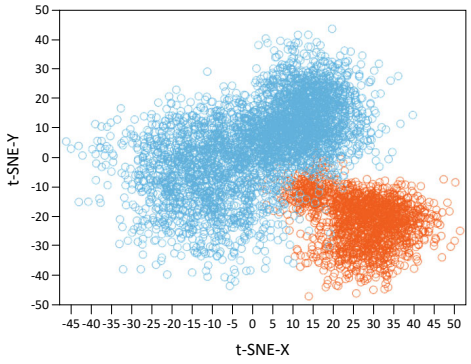

Figure 11. t-SNE projection of the features.

3.4 ECG Estimation

VibCardiogram targets to estimate the ECG waveform shape from the cardiogenic body vibrations collected from the wrist. These two signal types present the time-series cardiac activities in vibration and electrical domains, respectively. Using cardiogenic body vibrations to generate ECG waveform shapes is similar to translating a phrase from one language to another, which has nice solutions using the encoder-decoder-based methods.

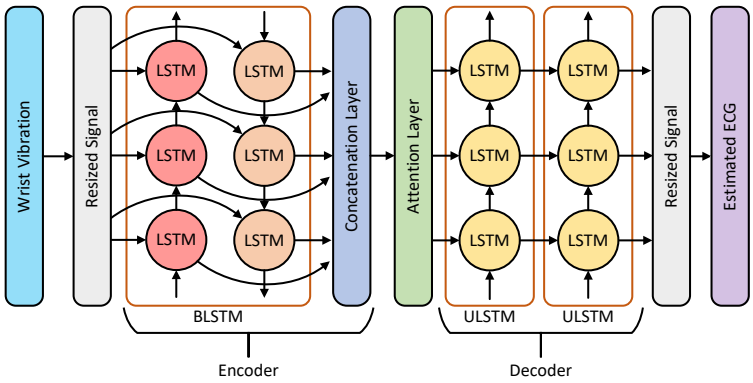

Fig. 12. The network structure of encoder-decoder model.

Therefore, we design an encoder-decode model to exploit the relationship between wrist vibration waveform shapes and ECG waveform shapes.

3.4.1 Encoder-Decoder Model Building. Fig. 12 shows the architecture of the encoder-decoder model. Generally, we choose Long Short Term Memory (LSTM) as the base network for our task. LSTM is a popular scheme for modeling time sequence data, and it has been successfully applied to physiology signal estimation [18, 84]. Specifically, the encoder is designed with a bidirectional LSTM (BLSTM) layer to extract fine-grained cardiac activity patterns in the wrist vibration signal. BLSTM is an extension to unidirectional LSTM (ULSTM), in which both the preceding and the following information are used to extract high-level descriptors of the wrist vibration signal. Given a T length input sequence $\tilde{x} = x_1, x_2, ..., x_T$, at each time step t, the LSTM reads x_t and updates the hidden state h_t by:

$$\begin{aligned} \overrightarrow{h_t} &= LSTM(x_t, \overrightarrow{h_{t-1}}), \\ \overleftarrow{h_t} &= LSTM(x_t, \overleftarrow{h_{t-1}}), \\ h_t &= \overrightarrow{h_t} \oplus \overleftarrow{h_t}, \end{aligned} \tag{3}$$

where the arrow represents the processing direction. The final output h_t of BLSTM is concatenated by the forward output $\overrightarrow{h_t}$ and the backward output $\overleftarrow{h_t}$. Note that the input vibration fragments have inconsistent lengths that vary from 0.6 s to 1 s. Thus, we resize the wrist vibration fragment into a 1.2 s sequence (120 samples) to obtain more accurate time-domain features. Such a process results in data with a fixed length but does not enrich the wrist vibration information. The output of BLSTM encodes the temporal features of cardiac activities and forms a contracting pathway in the feature space. Specifically, the encoder decreases the input signal to 1/4 of the original size (from 120 to 30).

The decoder is designed with two stacked ULSTM to form an expanding pathway (from 30 to 120), which interpolates the features learned from vibration waveform to ECG waveform. Then, we inversely resize the generated ECG into the same length as the original wrist vibration fragment. Although the encoder learns the general features related to cardiac activities, the down-sampling effect attenuates the fine details of the input. Some important cues for inferring ECG waveform shapes may be ignored.

To compensate for it, we bridge the encoder and decoder with an attention layer. The attention layer assigns weights to the encoder's hidden representation. The attention weight indicates the importance of the frame at time t to predict the output at time i. Therefore, the decoder will tend to the time steps with high weights. The

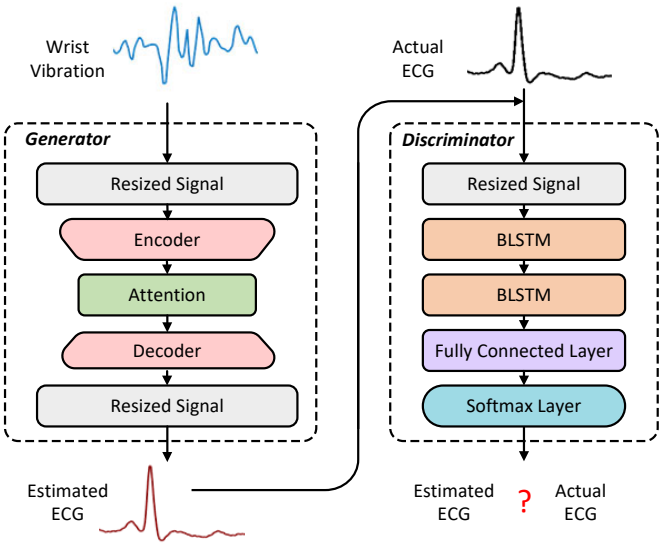

Fig. 13. The network structure combining GAN and encoder-decoder model.

weight is learned using a softmax layer:

$$\omega_{i,t} = \frac{exp(corr_{i,t})}{\sum exp(corr_{i,k})}, \tag{4}$$

where $corr_{i,t}$ computes the correlation coefficients between the hidden state s_{i-1} of the decoder and the hidden state h_t of the encoder, $corr_{i,t} = s_{i-1} \odot h_t$. The two hidden states with a strong correlation are probably associated with the same cardiac event. Finally, the output of the attention layer is calculated by $h_{att} = \sum \omega_{i,t} h_t$.

3.4.2 Encoder-Decoder Model Boosting. In the practical working scenario with a wrist-worn device, the vibration signal collection is impacted by many factors (e.g., sensing positions of the device). It will increase the collected waveform diversity and reduce the accuracy of the encoder-decoder model. To improve the performance, we develop a Generative Adversarial Networks (GAN)-based deep learning model to assist the training of the encoder-decoder model in an offline manner, which has been proven to be powerful for improving the system performance [22]. GAN as a framework to produce a model distribution that mimics a given target distribution, its practicality has been widely validated in several domain [34, 86]. GAN generally consists of a generator that produces new data and a discriminator that distinguishes the generated data from the real data. The concept is to consecutively train the generator and discriminator in turn, with the aim of reducing the difference between generated data and real data, meaning the generator model is generating plausible data.

Fig. 13 shows the architecture of the GAN-based deep learning model, which consists of a generator model and a discriminator model. Specifically, the generator is constructed as an encoder-decoder network, as presented above. With the great power of LSTM, the generator can learn the sophisticated mapping from the wrist vibration waveform shape to the ECG waveform shape. Then, the paired actual ECG waveform and ECG waveform estimated by the generator are resized into 120 length sequences and input into the discriminator. The discriminator judges whether the input ECG waveform is an actual ECG or estimated from a wrist vibration waveform. The discriminator is designed with two stacked BLSTM since the task is relatively light. With the fully connected layer and softmax layer, the discriminator outputs the probability that the current ECG waveform comes from the actual ECG waveform dataset.

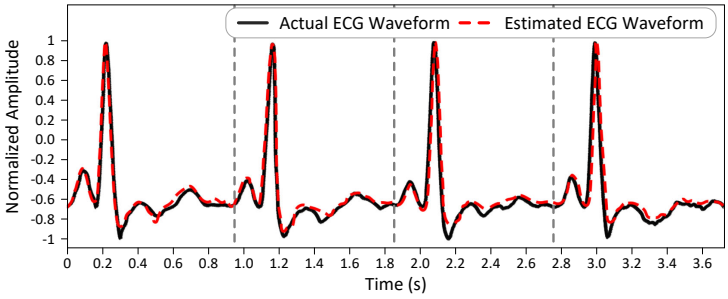

Fig. 14. An illustration of four adjacent ECG waveforms estimated by *VibCardiogram* and the corresponding actual ECG waveforms.

With the GAN architecture, the generator aims to fool the discriminator, while the discriminator aims not to be fooled by the generator model. During training, the parameters of both generator and discriminator are updated iteratively until the loss converges. Given a estimated ECG $\tilde{E} = \{E_1, E_2, ..., E_L\}$ and a actual ECG $\tilde{A} = \{A_1, A_2, ..., A_L\}$, the loss function of GAN model is formulated as the sum of estimation loss l_r and the adversarial loss l_a (i.e., $loss = l_r + l_a$). The estimation loss l_r is defined as

$$l_r = \frac{1}{L}\sum_{i=1}^{L}\frac{|A_i - E_i|}{A_i}, \tag{5}$$

and the adversarial loss l_a is defined as

$$l_a = log[1 - P_{EA}], \tag{6}$$

where P_{EA} is the probability that the discriminator recognizes the estimated ECG as actual ECG.

After training, the generator (encoder-decoder model) can convert the wrist vibrations waveform into ECG waveform accurately. Fig. 14 shows four adjacent ECG waveforms estimated by *VibCardiogram* compared to the corresponding actual ECG waveforms. It shows that the estimated ECG waveform is very close to the actual ECG waveform. Besides, we conduct an experiment to validate the effectiveness of the GAN model in boosting the estimation of ECG in Section 4.3.

Since the wrist vibrations are caused by the mass center of blood shifts in response to various cardiac activities, the relationship between ECG waveform and wrist vibrations could differ from one subject to another due to various factors, such as blood pressure, cardiac output, blood vessel elasticity, and body weight. These factors are hard to abstract and determine, we have tried to reduce their impact by dedicated training from multiple subjects, but the results receive insufficient accuracy (presented in Section 4.6). Therefore, we focus on building a user-specific model to achieve the desired accuracy.

4 EVALUATION

In this section, we first evaluate the overall performance of *VibCardiogram*. Then, we study the effectiveness of key algorithms and the impact of many factors (e.g., sampling rate and sensor position). Moreover, we study some practical issues, including *VibCardiogram*'s robustness against intense exercises, generalizability to new users in terms of estimating ECG waveforms and extracting HRV features, and long-term performance. Finally, we showcase an application of emotion recognition based on *VibCardiogram* to demonstrate its capability in supporting biosensing development.

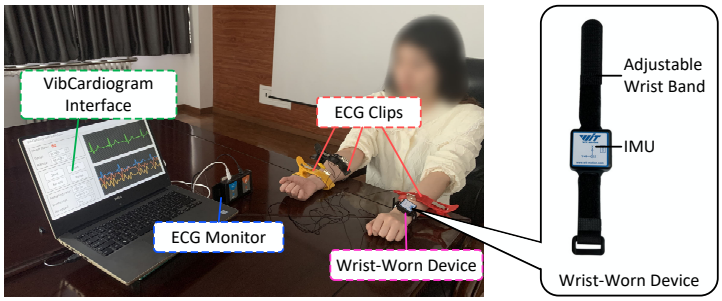

Fig. 15. Experimental setup and the wrist-worn prototype for evaluating the performance of *VibCardiogram*. A participant wears the wrist-worn prototype to collect wrist vibrations. Meanwhile, An ECG sensor with three clips are attached to the participant to obtain ground truth ECG.

4.1 Experiment Setup

4.1.1 Implementation. In our proof-of-concept implementation, we use Witmotion BWT901CL [1] watch to capture wrist vibration signals, as shown in Fig 15. This gadget has a similar appearance to a normal smartwatch (51.3 mm × 36 mm ×15 mm), can access the raw motion sensor reading and transmit the data to a remote server in real time, which simplifies the development of motion sensor-based applications on wearables. BWT901CL supports flexible control of the data sampling rate ranging from 20 Hz to 1000 Hz, which covers the sampling rate of most commercial devices. Specifically, we use the data from the axis in the same direction as the forearm for estimating ECG waveform shapes, as described in Section 2.3. Moreover, we develop the deep learning model using TensorFlow, Keras, and Sklearn.

4.1.2 Data Collection. There is no state-of-art dataset that simultaneously monitors ECG and wrist vibration from the wrist. Therefore, we collect our own dataset to implement and evaluate the system. The design does not seek to replace hospital equipment but renders a personal ECG waveform shape inferring system with prolonged recording time accessible to a larger sector of the population. The COVID-19 pandemic has made recruiting patients with cardiovascular diseases extremely difficult. Therefore, we recruit 20 participants (10 males, 10 females, ages 20-33) to conduct experiments for evaluating *VibCardiogram*. This study is conducted with the approval of our institute's ethics committee. All participants have no known medical conditions related to our evaluation. Fig. 15 shows the experimental setup for collecting data, which is conducted in a standard office building. During the data collection procedure, participants are asked to sit and wear the wrist-worn prototype. While gathering the wrist vibration data, the synchronized ground-truth ECG signals are collected by a custom AD8232 [2]-based ECG monitor that has proven to be accurate [25, 53] and is widely adopted by the research community to provide baseline [48, 87]. Overall, the dataset is collected for 30 minutes per participant. Moreover, to understand *VibCardiogram*'s performance against various factors, we collect data with various body movements, different sampling rates, and various sensor positions. Furthermore, we collect data under intense exercises to evaluate *VibCardiogram*'s robustness. Finally, to study *VibCardiogram*'s effectiveness in supporting downstream applications, we collect data while eliciting emotions.

4.1.3 Evaluation Methodology. To evaluate *VibCardiogram*, we define two metrics as follows,

(1) Estimation Error: the error between the estimated ECG E and actual ECG A compared to actual ECG A, which is defined as the same form of estimation loss in Equ. 5.

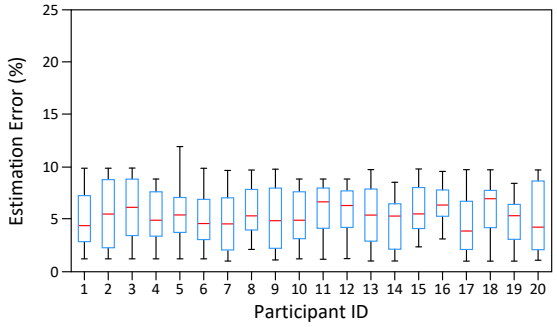

Fig. 16. Estimation error of 20 participants.

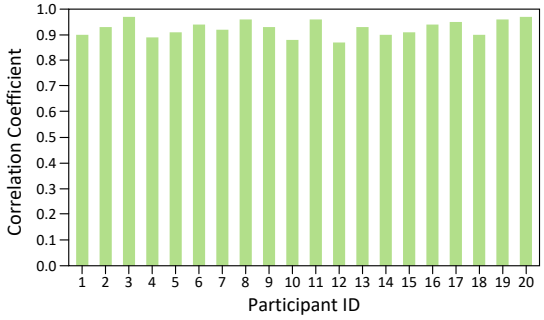

Fig. 17. Correlation coefficient of 20 participants.

(2) Correlation Coefficient: the shape similarity between estimated ECG E and actual ECG A, defined as

$$k = \frac{(E - \widetilde{E})(A - \widetilde{A})}{\sqrt{(E - \widetilde{E})^2}\sqrt{(A - \widetilde{A})^2}}, \tag{7}$$

where $\widetilde{E}$ and $\widetilde{A}$ represent the mean values of the estimated ECG E and actual ECG A, respectively.

4.2 Overall Performance

We first evaluate the overall performance of *VibCardiogram* for each participant respectively. Specifically, we use 75% data for training and the rest 25% data for testing, which is proven to be effective [13]. Fig. 16 shows the box plot of estimation error for each participant. The boxes are drawn from Q_1 (the median of the *lower* half of the dataset) to Q_3 (the median of the *upper* half of the dataset). The lowest point is the minimum estimation error, and the highest point is the maximum estimation error. Furthermore, the horizontal red line drawn in the middle represents the median. It can be observed that most errors are less than 10%. Overall, the average estimation error for all 20 participants is 5.989% with the standard deviation of 2.496%. According to American National Standards Institute, for the routine visual ECG readings, the tolerated average error for ECG amplitude is 10% [43]. Since our errors are within the acceptable margins, we can safely conclude that *VibCardiogram* achieves accurate ECG waveform reconstruction.

We also evaluate the correlation between the actual ECG waveform and the estimated ECG waveform. Fig. 17 shows the correlation coefficient for 20 participants. It can be observed that all participants receive correlation coefficients larger than 0.85. Overall, the average correlation coefficient is 0.926 with a standard deviation of 0.030. A correlation coefficient larger than 0.8 indicates a strong positive relationship. Therefore, we conclude that *VibCardiogram* can generate ECG highly related to the actual ECG waveform.

4.3 Key Algorithms Study

4.3.1 Effectiveness of Movement Noise Cancellation. To evaluate the effectiveness of our proposed movement noise cancellation algorithm, we ask participants to perform three different types of common movements fifty times each: walking (whole-body movement), interacting with a smartphone (near-wrist movement), and moving the back arm (far-wrist movement). The estimation error (shown in Fig. 18(a)) and correlation coefficient (shown in Fig. 18(b)) are compared between without and with applying the proposed method. In particular, we segment the wrist vibration signals according to the ground truth ECG, because movement noise can cause significant segmentation errors. When applying the algorithm, it can be observed that the estimation error decreases significantly, and the correlation coefficient increases significantly. Although near wrist movement has the

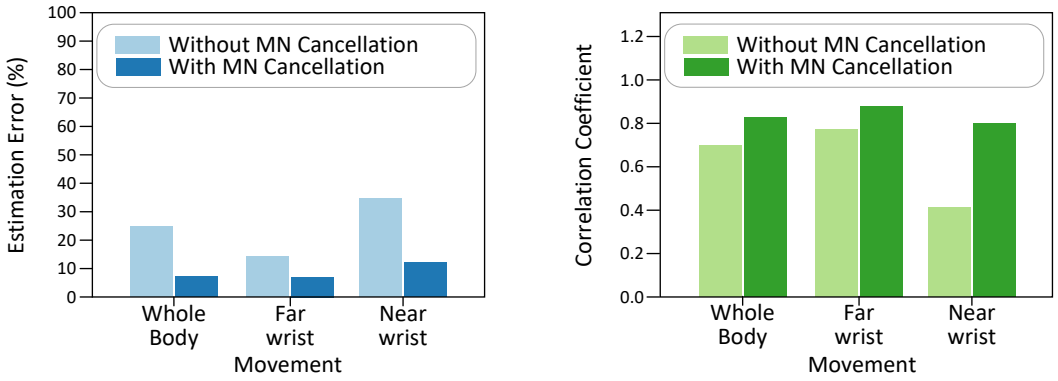

(a) Estimation error (b) Correlation coefficient

Fig. 18. System performance without and with applying the movement noise (MN) cancellation method.

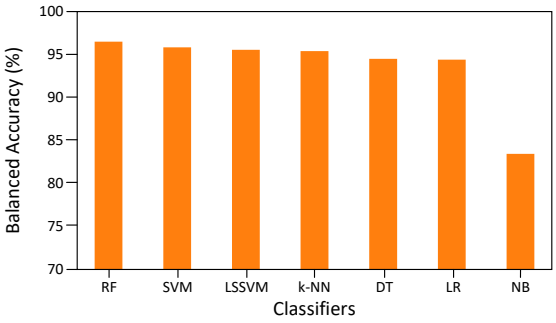

Fig. 19. Impact of machine learning classifiers.

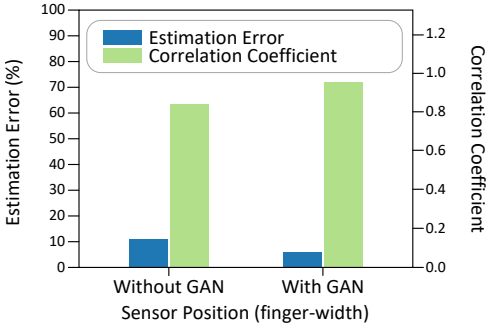

Fig. 20. Correlation coefficient of 20 participants.

greatest negative impact on the system performance, *VibCardiogram* can achieve acceptable results after applying the movement noise cancellation algorithm. Overall, after noise cancellation, the average estimation error is 8.819%, and the average correlation coefficient is 0.833. The result implies that *VibCardiogram* is practical for daily life usage. Furthermore, we evaluate *VibCardiogram*'s robustness against intense exercise in Section 4.5.

4.3.2 Impact of Machine Learning Methods for Vibration Signal Segmentation. The core of segmentation is to identify the troughs corresponding to ventricular systole. We study the performance of spike point identification with different machine learning methods. Specifically, seven commonly used classifiers are implemented, including Random Forest (RF), Support Vector Machine (SVM), Least Squares Support Vector Machine (LSSVM), k-Nearest Neighbors (k-NN), Decision Trees (DT), Logistic Regression (LR), and Naive Bayes (NB). In Fig. 19, we show the balanced accuracy (BAC) of different classifiers. BAC is calculated as $BAC(y, \hat{y}) = \frac{1}{2}\sum_{i=1}^{2}\sum_{j=1}^{m_i} 1(\hat{y}_{i,j} = y_{i,j})/m_i$, where y and $\hat{y}$ represent the true condition and predicted condition of candidate points, respectively, and m is the number of points belonging to each class (i.e., actual spike points and other points). We can observe that RF receives the highest balanced accuracy of 96.6% and is adopted in this work.

4.3.3 Effectiveness of GAN on Boosting the ECG Estimation Model. We develop the GAN to boost accurate estimation of ECG waveform shapes. We compare the ECG estimation model (the encoder-decoder model) trained by GAN to the same model trained without GAN. In particular, without GAN, the ECG estimation model is trained by minimizing the estimation loss. We summarize the estimation error and correlation coefficient in Fig. 20. The results are averaged across 20 participants. Clearly, GAN can significantly reduce the estimation error

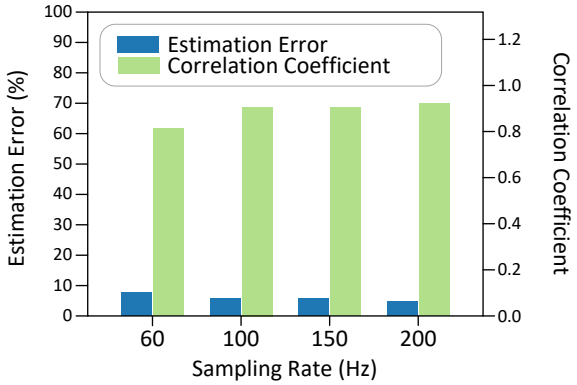

Fig. 21. Impact of sampling rate.

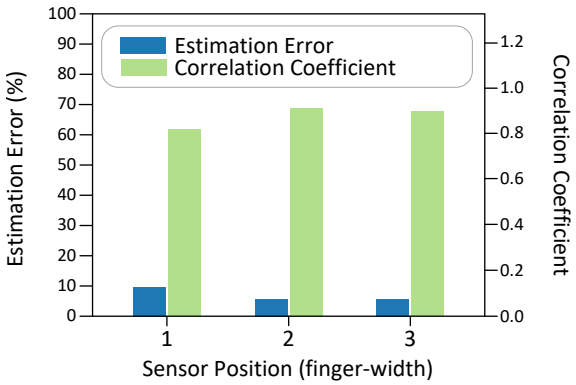

Fig. 22. Impact of sensor position.

and increase the correlation coefficient. This validates the effectiveness of GAN in boosting the ECG estimation model.

4.4 Impact Factors

4.4.1 Impact of Sampling Rate. On the one hand, a high sampling rate enables capturing detailed information about wrist vibration but increases computational cost. On the other hand, a low sampling rate loses some fine-grained information and may further degrade the system performance. To understand the impact of sampling rate on *VibCardiogram*, we ask participants to collect data with four sampling rates (60 Hz, 100 Hz, 150 Hz, and 200 Hz) for thirty minutes each. Fig. 21 compares the results of four sampling rates. It can be seen that *VibCardiogram* performs better when the sampling rate increases. Besides, all sampling rates receive estimation error smaller than 10% and correlation coefficient larger than 0.8. Moreover, the result suggests that *VibCardiogram* can obtain acceptable results with a limited sampling rate.

4.4.2 Impact of Sensor Position. The sensor position is one of the critical impact factors affecting the captured wrist vibration pattern. Thus, we study the performance of *VibCardiogram* with different sensor positions. We ask participants to wear the smartwatch 1, 2, and 3 finger-widths above their wrist bone and collect data for thirty minutes each. In Fig. 22, we show the average waveform estimation error and average correlation coefficient across 20 participants. Despite that sensor position affects the system performance, *VibCardiogram* realizes an average estimation error smaller than 10% and an average correlation coefficient larger than 0.8. The result suggests that *VibCardiogram* is robust at different positions.

4.5 Exercise-Robustness

As a follow-up to the previous experiment on movement-robustness in daily life usage, we also are interested in measuring how well *VibCardiogram* performs during intense exercises. To evaluate the robustness of *VibCardiogram* under intense exercises, we ask all participants to collect wrist vibrations while performing anaerobic exercises, including dumbbell bench press and cable biceps curl, and aerobic exercises, including stationary biking and elliptical. We consider these exercises because they introduce interference in sensor data and change the cardiac rhythm, while still enabling true ECG monitoring (true ECG signals collected under movements such as running and jumping are fully contaminated by movement noise, thus running and jumping are not considered). Particularly, we manually check the collected ground truth ECG signals and discard those segments that contain errors. And we only keep data with heart rate above 140 beats/min to better study the effect of intense exercise on the system's performance. In total, we obtain over 230 min of data for the four types of exercises.

We carefully evaluate *VibCardiogram*' performance under intense exercises with three different experimental setting cases: (i) The training data are from normal states and the testing data are from exercise; (ii) The evaluated dataset only includes data under exercise, and data of four types of exercises are mixed together then randomly split into 75% for training and 25% for testing; (iii) The data under exercise are divided into four exercise-specific datasets grouped by exercise type. Each dataset is evaluated separately by splinting 75% data for training and 25% data for testing. Fig. 23 reports the results in different cases. We find case i receives an average estimation error of around 40% and an average correlation coefficient below 0.6, which is not enough to guarantee effective reconstruction of ECG waveform. This is because exercises not only cause significant noise in the sensor data but also change the cardiac rhythm and subsequently distort the true ECG waveform shape. Compared to normal states, exercises would cause a decrease in magnitudes of QRS complex and T wave, deviation in the right axis, and junctional depression of the ST segment [72, 73]. Moreover, case ii has a 25.457% estimation error and 0.718 correlation coefficient. The correlation coefficient is above 0.6, indicating a moderate positive relationship between the generated ECG waveform and the true ECG waveform. However, the results suggest that the mixed training set from multiple exercise types is still not sufficient to build an exercise-robust system. Encouragingly, an improvement in performance can be noticed in case iii, which shows that the exercise-specific dataset is expected to handle the wide spectrum of human behavior under exercise. The study of more exercises is left as future work.

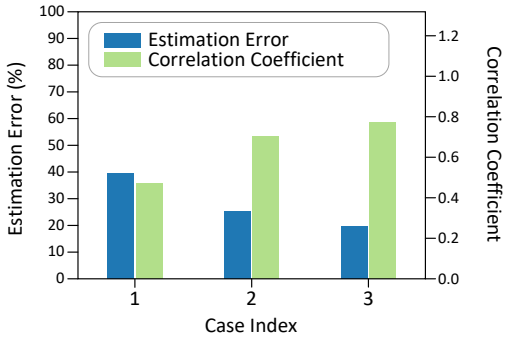

Figure 23. System performance under intense exercises, evaluated in three experimental setting cases.

Table 3. Time domain, frequency domain, and non-linear (Poincaré plot) features of HRV. Adapted from [51, 52, 56, 78].

Domain	Index	Features
Time	1	Standard deviation of all interbeat intervals
	2	Ratio of thestandard deviation and mean of interbeat intervals
	3	The number of paris of adjacent interbeat intervals that more than 50ms
Frequency	4	Low frequency power (0.04-0.15Hz)
	5	High frequency power (0.15-0.4Hz)
	6	Ratio of the low-to-high frequency power
Poincaré plot	7	Short-term beat-to-beat variability
	8	Long-term beat-to-beat variability

4.6 Generalizability

We evaluate whether the system can generalize to new users without retraining, i.e., the robustness of *VibCardiogram* against individual differences. We conduct leave-one-participant-out validation, using data from one participant for testing and the remaining 19 participants for training. The results are calculated from all 20 combinations for testing and training data. We first report the waveform estimation performance. Moreover, we present how accurate *VibCardiogram* is in estimating HRV features by inputting the reconstructed signal to PhysioNet Cardiovascular Signal Toolbox [80]. Table 3 summarizes the considered HRV features, which is adapted from [51, 52, 56, 78].

Fig. 24 reports the ECG waveform estimation performance for each participant. Overall, *VibCardiogram* achieves 22.275% estimation error with 13.125% standard deviations and achieves a correlation coefficient of 0.656. On the plus side, we find that 13 of the 20 participants have correlation coefficients above 0.6, and participant 12 even receives a correlation coefficient above 0.8. The results confirm *VibCardiogram* has certain effectiveness in user-independent scenarios. Some users may use *VibCardiogram* directly without the trouble of providing

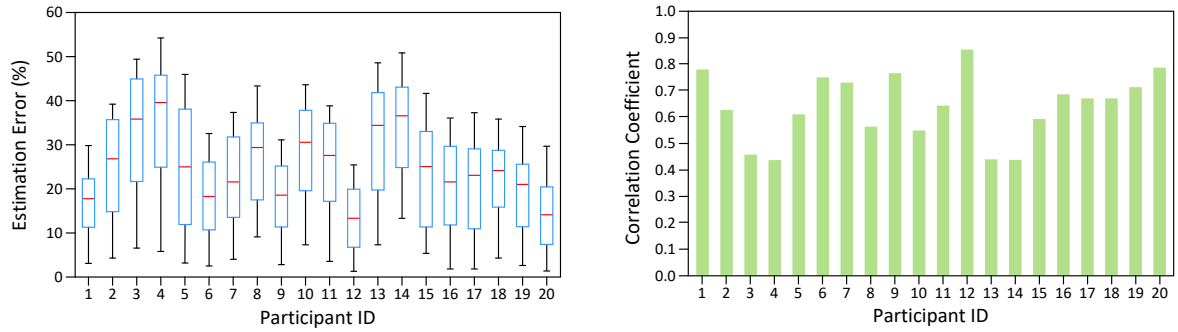

(a) Estimation error (b) Correlation coefficient

Fig. 24. System robustness against individual differences in estimating ECG waveform shapes.

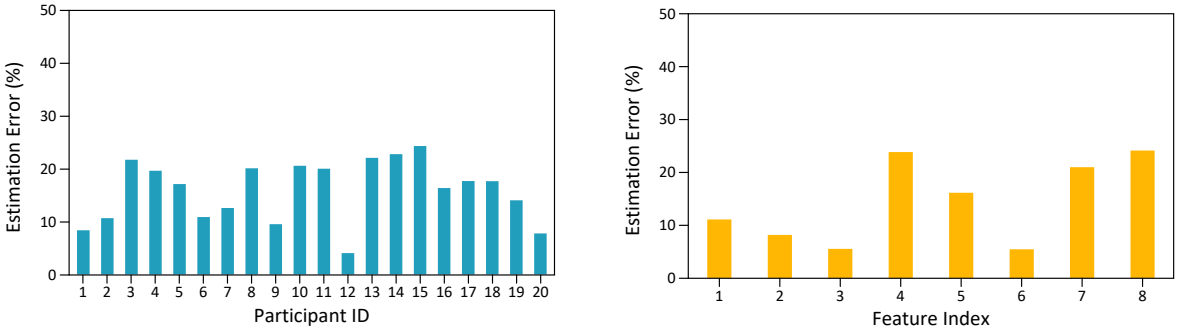

(a) Estimation error for each participant (b) Estimation error for each feature

Fig. 25. System robustness against individual differences in extracting HRV features.

training data. On the minus side, we notice some participants obtain correlation coefficients lower than 0.5, indicating that they could not directly use the system without providing training data.

Besides correlation, we quantify the effectiveness of *VibCardiogram* by the estimation errors for extracting HRV features. We report the estimation error for extracting HRV features for each user in Fig. 25(a), where the overall estimation error respect to the average true feature value (obtained from true ECG waveform using the PhysioNet Cardiovascular Signal Toolbox) averaged across all features is 14.53%. We then analyze the results for each feature in Fig. 25(b) (The same results in Fig. 25(a) but re-grouped according to features). On the upside, we find that 15 of 20 participants obtain estimation errors lower than 20%. Besides, time-domain HRV features and the ratio of the low-to-high frequency power are almost immune to individual differences, and achieve low estimation error in a user-independent manner. In particular, we observe that the main error in ECG waveform shape estimation for most participants comes from amplitude error, which has a limited impact on estimating the HRV features. On the downside, we notice participants 3, 13, and 14 have relatively poor performance when directly using *VibCardiogram*. After carefully studing the results, we find that their body vibrations differ significantly from other participants. Consequently, the shapes of their generated signal waveform are also different from the standard ECG waveform shape, which causes high estimation errors for estimating HRV features. Overall, the above results suggest that *VibCardiogram* has certain generalizability but the current encoder-decoder model is still insufficient to work across all new users. Moreover, *VibCardiogram* has good generalizability for extracting certain types of HRV features, presenting promising potentials for downstream healthcare applications.

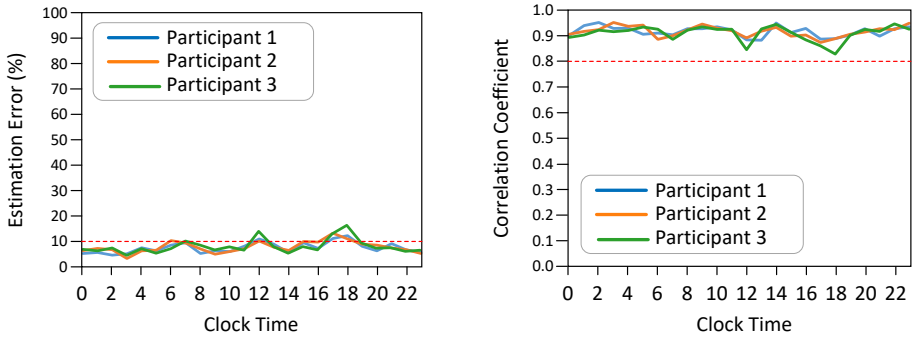

(a) Estimation error (b) Correlation coefficient

Fig. 26. 24-hour performance.

4.7 Long-Term Performance

We ask three participants to wear the prototype and collect continuous wrist vibration data and ground truth ECG for 24 hours in our lab. We encourage them to perform daily activities during the experiment. Fig. 26(a) and Fig. 26(b) show the 24-hour estimation error and correlation coefficient, respectively. The results are averaged every hour. Overall, the average estimation errors of the three participants are 7.675%, 7.98%, and 8.25%, respectively. The average correlation coefficient are 0.916, 0.916, and 0.909, respectively. The result suggests that *VibCardiogram* is promising to facilitate long-term ECG waveform shape estimation. Besides, we can observe that participant 3 during 12, and 18 o'clock receives relatively high estimation errors. One possible reason is that the participant eats and performs a lot of near-wrist movements during these periods. The study of this special case is left as future work.

4.8 Using *VibCardiogram* for Emotion Recognition

We now showcase the usefulness of *VibCardiogram* by investigating an application of extracting HRV features then recognizing state-of-emotion; we investigate this one because it appears to be one of the most popular sensing tasks in recent publications [66, 87]. We consider four types of emotions, including happy, sad, anger, and fear. To induce emotions, we prepare four types of movie clips for four emotions, each lasting for 10 minutes. The movie clips method has been proved effective for emotion induction by existing studies [28, 29]. We ask the participants to watch all movie clips in a random sequence for five sessions to induce emotions meanwhile collecting wrist vibration data. Between clips and between sessions, we play an additional 1 min relax movie clip to ensure the independence of emotions. In total, we collect 20×5×10×4min wrist vibration data. Based on the collected data, *VibCardiogram* profiles the wrist vibrations and estimate the corresponding ECG waveform.

We realize emotion recognition through the pipeline of HRV extraction, Principal Component Analysis (PCA)-based feature selection, and classification, matching that considered in [29]. We first divide the ECG waveform sequence into 1min non-overlapping segments and extract typical HRV features from each segment as described in Section 4.6. Then we select five significant features with high Eigen values using PCA, including features indexed 2, 4,5,6, and 7. Finally, we arrange the five features into a feature vector and input the vector to a classifier for emotion recognition. With the number of different prediction methods, we implement several highly used classifiers, including linear kernel SVM, k-NN, RF, DT (all with default settings). In the experiment, we split the collected data into 75% training data and 25% testing data, and use the Correct Classification Rate (CCR) to evaluate our system. Overall, SVM achieves 71% CRR, RF achieves 67% CRR, DT achieves 61% CRR, and kNN achieves 58% CRR. Table 4 compares our performance with typical emotion recognition approaches using commodity ECG devices. We notice that our method achieves comparable performance with these related works. Therefore, we

Table 4. Comparison of our method with typical existing methods in emotion recognition.

Work	Stimuli	Modalities	Emotional Annotations	CCR
[41]	Multimodal	ECG, SKT, EDA	Sad, anger,stress,supprise	78.4%
[64]	Pirturing viewing	ECG, EMG, RSP, EDA	Happy, disgust, fear	62.70%
[40]	Music	ECG, EMG, RSP	Happy, anger, sad, pleasure	69.70%
[81]	Video clips	ECG, OXY, GSR	Anusement, anger, grief, fear, baseline	74.00%
Our method	Video clips	ECG	Happy, sad, anger, and fear	71.00%

SKT: skin temperature; EDA: electrodermal activity; EMG: electromyogram; RSP: respiration features; GSR: galvanic skin response; OXY: blood oxygen saturation.

can safely conclude that the ECG waveform generated by *VibCardiogram* is effective for extracting HRV features and further enable accurate emotion recognition. Moreover, this confirms the usefulness of *VibCardiogram*, and we plan to explore versatile sensing applications (e.g., HRV analysis [78], detect driver fatigue [71], verify user's identity [6], and sleep stage monitoring [21].) in the future.

5 RELATED WORK

Conventional ECG monitoring techniques generally use wet electrodes attached to the skin to capture ECG signals [43]. However, they require sticky gels and may cause skin irritation during the recording. Moreover, they are expensive (>$10,000) and need to be operated by professionals, which is not preferred for daily use.

With recent advances in sensing technology, new solutions for daily ECG monitoring have emerged. Smart household facilities have increased as they support comfortable and easy-to-use monitoring of ECG, including beds [59], toilet seats [42], chairs [50] and ceiling-mounted microwave sensors [85]. However, their usefulness is realistically restricted to limited scenarios (e.g., when sitting on a chair or lying on the bed). Besides, because these systems do not support long-term ECG monitoring, infrequent heart problems, such as premature beats and heart arrhythmia, cannot be effectively detected.

To facilitate ECG monitoring in ubiquitous environments, portable and wearable devices are developed. Several works have looked at using flexible fabric electrodes embedded in textiles (e.g., smart garments [37] and belts [62]). However, they require special hardware with high costs and complicated setup, which are usually unaffordable to the common person. Apple Watch [4] and Samsung Galaxy Watch [3] include dry ECG electrodes on their devices to support ECG monitoring. However, they require users to press fingers on the ECG pad throughout data collection. Since the finger pulse oximeter can capture signals that contain information about heart beating patterns, researchers have explored inferring ECG signals using finger pulse oximeters [16, 77, 89]. However, the use of finger-worn devices is inconvenient and intrusive to daily living and the body. Besides, pulse oximeters are particularly susceptible to body movements, skin tone diversity, and various ambient light intensities. Therefore, these methods are not accurate in real-world situations. Our work is closely related to Biowatch [30], which infers the heart rate using wearable motion sensors. The main difference between our design and Biowatch is that we can obtain the fine-grained ECG waveform, while Biowatch only obtains a cardiac parameter. The estimation of heart rate is not sufficient for detecting many serious cardiovascular diseases.

Compared with prior works, *VibCardiogram* only relies on motion sensors available on wrist-worn devices, which are affordable and easy to use. It can effectively address the noise caused by daily activities and obtain accurate ECG measurements. Besides, it does not require any particular behavior changes and does not disturb users. Thus, it is suitable for long-term use (i.e., enable anywhere anytime monitoring). In summary, to the best of our knowledge, our work is the first to enable an alternative solution for accurate, low-cost, passive, non-intrusive, and convenient ECG waveform shape estimation from wearable motion sensors.

6 DISCUSSION AND FUTURE WORK

In this section, we discuss the limitations of *VibCardiogram*, the possible improvements, and the directions for further investigation. Firstly, we implement *VibCardiogram* with the wrist-worn IMU-based sensing platform Witmotion BWT901CL for flexible configuration and rapid evaluation. We acknowledge that such a platform has more stable sampling, higher sensitivity, etc., compared to a real commercial smartwatch. To make *VibCardiogram* applicable to commercial smartwatches, we devise several techniques to ensure a fixed sampling rate and reliable measurements. We plan to explore the performance of *VibCardiogram* using multiple main smartwatches, which would further confirm the effectiveness of our design.

Secondly, we only evaluate *VibCardiogram* with healthy subjects recruited from friends and colleagues. Therefore, *VibCardiogram*'s effectiveness is confined to support biosensing applications for healthy users. We are aware that cardiovascular diseases would affect heart functions, thereby distorting the generated ECG waveform. For example, the ECG waveform shows chaotic irregular deflections of varying amplitudes in the case of ventricular fibrillation. And sometimes, P waves, QRS complexes, or T waves can be not identifiable [10]. It is worth investigating *VibCardiogram*'s performance for supporting biosensing applications [82] with diagnosed patients with cardiovascular diseases. Moreover, *VibCardiogram* is expected to fuel versatile medical-related applications for the diagnosis of many diseases. We are discussing with local medical institutions to put *VibCardiogram* into use, so that we may gather more performance results from diagnosed patients. On the positive side, results presented in Section 4 demonstrate that *VibCardiogram* has certain robustness. Thus the generated ECG waveform may retain some characteristics of the true ECG waveform. Besides, errors in ECG waveforms do not necessarily cause errors in downstream applications. Therefore, we believe that by updating the training dataset and retraining the system model, *VibCardiogram* is excepted to resolve the mapping between cardiogenic body vibration and ECG waveform to some extent.

Thirdly, we have not seriously evaluated the effect of device wearing states. Prior studies suggest that the device wearing state could affect the sensor readings of the smartwatch [55]. For example, when the smartwatch is loosely attached to the skin, cardiogenic body vibrations may not be strong enough to cause significant fluctuations in the IMU readings, and body movements would introduce noise to the sensor data. Luckily, a lot of research efforts have been made to profile the device wearing states. For example, by exploiting the PPG sensor widely deployed on smartwatches, the contact pressure between the smartwatch and the wrist skin can be profiled using the least-squares support vector machine [12]. In addition to automatically characterizing the device wearing states to ensure the tracking usability, we suggest the users wear the smartwatch on the wrist from 1-2 finger-widths away from the wrist bone, matching the position recommended by popular smartwatches [74, 83].

Fourthly, we have demonstrated that *VibCardiogram* is accurate when the model is trained user-specific. We are yet to add data from more people to the training dataset to improve system robustness with variable situations and to ease the enrollment effort. However, the experiment in Section 4.6 indicates different users exhibit different data characteristics. Adding data from a large amount of other users' data may "curse" the system and make some users obtain inaccurate prediction results. Future research will carefully evaluate the impact of different dataset combinations, which could help us to improve system performance.

Fifthly, while we have demonstrated that *VibCardiogram* can achieve user-independent for extracting certain HRV features and be directly used by some new users, its generalizability is still limited due to the diverse cardiovascular functions. A user-independent system is more desirable, and we seek to approach this in the future. A potential solution is to manually enter some personal information in the model (e.g., body weight, age, gender), mine the general information using data collected from a large number of people, and apply transfer learning, which has shown initial success in build a user-independent blood pressure monitoring system [12].

Last but not least, *VibCardiogram*'s pipeline currently focuses on motion-robustness in daily life usage, where the users keep normal heart rates. The experiment in Section 4.3.1 confirms that *VibCardiogram* accurately

recovers the ECG waveform under body movements such as walking and moving arms. Since ECG monitoring during exercise has drawn significant attention for versatile applications, we are also interested in measuring *VibCardiogram*'s performance during exercise. However, exercise not only causes interference in the sensor data, but also speeds up heart rate and increases stroke volume, thereby affecting the true ECG waveform shapes. The experiment in Section 4.5 demonstrates that *VibCardiogram* currently is not enough to build an exercise-robust system. But the results show positive signs that building a training dataset for specific exercises would improve the overall system performance. We are planning to gather more training with exercise-specific datasets. Moreover, we are planning to explore more advanced techniques that are proven to resist intense activities, such as spectral subtraction, time-frequency analysis [24], and piezoelectric transducer-based method [45], to approach exercise-robustness.

7 CONCLUSION

This paper serves as the first step towards a comprehensive understanding of motion sensor-based ECG waveform shape reconstruction. We propose a novel system, *VibCardiogram*, which uses low-cost motion sensors available in ubiquitous wrist-worn devices (e.g., smartwatches and fitness trackers). It works by profiling wrist vibrations produced by cardiac activities and transforming the wrist vibrations waveforms into accurate ECG waveforms. We develop a novel algorithm that can effectively disentangle wrist vibration caused by heart beating from noisy motion sensor data. Besides, we propose a segmentation method that can tackle the waveform variety of individual vibration beats. Moreover, we design a deep learning architecture based on encoder-decoder and GAN to generate an accurate ECG waveform. Overall, *VibCardiogram* obtains an average estimation error of 5.989%, which is within the acceptable range regulated by the American National Standards Institute. Besides, *VibCardiogram* achieves an average correlation of 0.926, suggesting the estimated ECG waveforms are strongly correlated to the true ECG waveforms. Moreover, we showcase its ability to extract HRV features and support downstream applications. The promising results make us believe that the release of *VibCardiogram* can greatly reshape the daily experience of mobile ECG waveform shape estimation and advance ECG-based applications.

ACKNOWLEDGMENTS

The work of Fan Li is partially supported by the National Natural Science Foundation of China (NSFC) under Grant No. 62072040. The work of Huijie Chen is partially supported by China Postdocporal Science Foundation under Grant No. 2021M700302. The work of Li Zhang is partially supported by NSFC under Grant No. 61972131.

REFERENCES

[1] 2020. Witmotion BWT901. https://github.com/WITMOTI-ON/BWT901
[2] 2022. AD8232 Heart Rate Monitor Guide. https://learn.sparkfun.com/tutorials/ad8232-heart-rate-monitor-hookup-guide/all
[3] 2022. ECG at Your Fingertips. https://www.samsung.com/us/apps/samsung-health-monitor/
[4] 2022. Record an ECG on Apple Watch. https://support.apple.com/en-us/HT208955
[5] Rashid Ghorbani Afkhami, Ghanbar Azarnia, and Mohammad Ali Tinati. 2016. Cardiac Arrhythmia Classification Using Statistical and Mixture Modeling Features of ECG Signals. *Pattern Recognition Letters* 70 (2016), 45–51.
[6] Juan Sebastian Arteaga-Falconi, Hussein Al Osman, and Abdulmotaleb El Saddik. 2015. ECG Authentication for Mobile Devices. *IEEE Transactions on Instrumentation and Measurement* 65, 3 (2015), 591–600.
[7] Roman M Baevsky and Anna G Chernikova. 2017. Heart Rate Variability Analysis: Physiological Foundations and Main Methods. *Cardiometry* 10 (2017).
[8] Kim E Barrett, Scott Boitano, Susan M Barman, and Heddwen L Brooks. 2010. Ganong's Review of Medical Physiology Twenty. (2010).
[9] Luca Bergamaschi, Emanuela Concetta D'Angelo, Pasquale Paolisso, Sebastiano Toniolo, Michele Fabrizio, Francesco Angeli, Francesco Donati, Ilenia Magnani, Andrea Rinaldi, Lorenzo Bartoli, et al. 2021. The Value of ECG Changes in Risk Stratification of COVID-19 Patients. *Annals of Noninvasive Electrocardiology* 26, 3 (2021), e12815.
[10] Selcan Kaplan Berkaya, Alper Kursat Uysal, Efnan Sora Gunal, Semih Ergin, Serkan Gunal, and M Bilginer Gulmezoglu. 2018. A Survey on ECG Analysis. *Biomedical Signal Processing and Control* 43 (2018), 216–235.

[11] Amelie Bonde, Shijia Pan, Zhenhua Jia, Yanyong Zhang, Hae Young Noh, and Pei Zhang. 2018. VVRRM: Vehicular Vibration-Based Heart RR-Interval Monitoring System. In *Proc. of the 19th ACM HotMobile*. 37–42.

[12] Yetong Cao, Huijie Chen, Fan Li, and Yu Wang. 2021. Crisp-BP: Continuous Wrist PPG-Based Blood Pressure Measurement. In *Proc. of the 27th ACM MobiCom*. 378–391.

[13] Yetong Cao, Qian Zhang, Fan Li, Song Yang, and Yu Wang. 2020. PPGPass: Nonintrusive and Secure Mobile Two-Factor Authentication via Wearables. In *IEEE INFOCOM 2020-IEEE Conference on Computer Communications*. 1917–1926.

[14] Ayan Chatterjee and Uttam Kumar Roy. 2018. Non-Invasive Heart State Monitoring an Article on Latest PPG Processing. *Biomedical and Pharmacology Journal* 11, 4 (2018), 1885–1893.

[15] MPS Chawla. 2011. PCA and ICA Processing Methods for Removal of Artifacts and Noise in Electrocardiograms: A Survey and Comparison. *Applied Soft Computing* 11, 2 (2011), 2216–2226.

[16] H. Y. Chiu, H. H. Shuai, and C. P. Chao. 2020. Reconstructing QRS Complex From PPG by Transformed Attentional Neural Networks. *IEEE Sensors Journal* 20, 20 (2020), 12374–12383.

[17] Louise V Coutts, David Plans, Alan W Brown, and John Collomosse. 2020. Deep Learning With Wearable Based Heart Rate Variability for Prediction of Mental and General Health. *Journal of Biomedical Informatics* 112 (2020), 103610.

[18] Debashis Das Chakladar, Shubhashis Dey, Partha Pratim Roy, and Debi Prosad Dogra. 2020. EEG-Based Mental Workload Estimation Using Deep BLSTM-LSTM Network and Evolutionary Algorithm. *Biomedical Signal Processing and Control* 60 (2020), 101989.

[19] Thomas P Davis, Jay Alexander, and Michael Lesch. 1993. Electrocardiographic Changes Associated With Acute Cerebrovascular Disease: A Clinical Review. *Progress in Cardiovascular Diseases* 36, 3 (1993), 245–260.

[20] Denis Doyen, Pamela Moceri, Dorothée Ducreux, and Jean Dellamonica. 2020. Myocarditis in a Patient With COVID-19: A Cause of Raised Troponin and ECG Changes. *The Lancet* 395, 10235 (2020), 1516.

[21] Pedro Fonseca, Xi Long, Mustafa Radha, Reinder Haakma, Ronald M Aarts, and Jérôme Rolink. 2015. Sleep Stage Classification with ECG and Respiratory Effort. *Physiological measurement* 36, 10 (2015), 2027.

[22] Yang Gao, Yincheng Jin, Jagmohan Chauhan, Seokmin Choi, Jiyang Li, and Zhanpeng Jin. 2021. Voice In Ear: Spoofing-Resistant and Passphrase-Independent Body Sound Authentication. *Proc. of ACM IMWUT 2021* 5, 1, Article 12 (March 2021), 25 pages.

[23] Shkurta Gashi, Elena Di Lascio, and Silvia Santini. 2019. Using Unobtrusive Wearable Sensors to Measure the Physiological Synchrony Between Presenters and Audience Members. *Proc. of the ACM on Interactive, Mobile, Wearable and Ubiquitous Technologies* 3, 1, Article 13 (mar 2019), 19 pages.

[24] Andrea Gentili, Alberto Belli, Lorenzo Palma, Salih Murat Egi, and Paola Pierleoni. 2019. A Real-Time Algorithm for PPG Signal Processing During Intense Physical Activity. In *EAI International Conference on IoT Technologies for HealthCare*. 22–36.

[25] Muhammad Wildan Gifari, Hasballah Zakaria, and Richard Mengko. 2015. Design of ECG Homecare: 12-Lead ECG Acquisition Using Single Channel ECG Device Developed on AD8232 Analog Front End. In *Proc. of IEEE ICEEI 2015*. 371–376.

[26] Laurent Giovangrandi, Omer T Inan, Richard M Wiard, Mozziyar Etemadi, and Gregory TA Kovacs. 2011. Ballistocardiography—a Method Worth Revisiting. In *Proc. of IEEE IWMBS 2011*. IEEE, 4279–4282.

[27] J. W. Gordon. 1877. Certain Molar Movements of the Human Body Produced by the Circulation of the Blood. *Journal of Anatomy & Physiology* 11, Pt 3 (1877), 533.

[28] James J Gross and Robert W Levenson. 1995. Emotion Elicitation using Films. *Cognition & Emotion* 9, 1 (1995), 87–108.

[29] Han-Wen Guo, Yu-Shun Huang, Chien-Hung Lin, Jen-Chien Chien, Koichi Haraikawa, and Jiann-Shing Shieh. 2016. Heart Rate Variability Signal Features for Emotion Recognition by Using Principal Component Analysis and Support Vectors Machine. In *Proc. of the 16th IEEE BIBE*. 274–277.

[30] Javier Hernandez, Daniel McDuff, and Rosalind W. Picard. 2015. BioWatch: Estimation of Heart and Breathing Rates From Wrist Motions. In *Proc. of the 9th IEEE PervasiveHealth*. 169–176.

[31] Yu-Liang Hsu, Jeen-Shing Wang, Wei-Chun Chiang, and Chien-Han Hung. 2017. Automatic ECG-Based Emotion Recognition in Music Listening. *IEEE Transactions on Affective Computing* 11, 1 (2017), 85–99.

[32] Omer T Inan, Pierre-Francois Migeotte, Kwang-Suk Park, Mozziyar Etemadi, Kouhyar Tavakolian, Ramon Casanella, John Zanetti, Jens Tank, Irina Funtova, G Kim Prisk, et al. 2014. Ballistocardiography and Seismocardiography: A Review of Recent Advances. *IEEE Journal of Biomedical and Health Informatics* 19, 4 (2014), 1414–1427.

[33] M Jagannath and Venkatesh Balasubramanian. 2014. Assessment of Early Onset of Driver Fatigue Using Multimodal Fatigue Measures in a Static Simulator. *Applied ergonomics* 45, 4 (2014), 1140–1147.

[34] Hyejeong Jeong, Jieun Yu, and Wonjun Lee. 2021. A Semi-Supervised Approach for Network Intrusion Detection Using Generative Adversarial Networks. In *IEEE INFOCOM 2021-IEEE Conference on Computer Communications Workshops (INFOCOM WKSHPS)*. IEEE, 1–2.

[35] Zhenhua Jia, Amelie Bonde, Sugang Li, Chenren Xu, Jingxian Wang, Yanyong Zhang, Richard E Howard, and Pei Zhang. 2017. Monitoring a Person's Heart Rate and Respiratory Rate on a Shared Bed Using Geophones. In *Proc. of the 15th ACM SenSys*. 1–14.

[36] Chandrakar Kamath. 2011. ECG Beat Classification Using Features Extracted From Teager Energy Functions in Time and Frequency Domains. *IET Signal Processing* 5, 6 (2011), 575–581.

[37] Nazmul Karim, Shaila Afroj, Andromachi Malandraki, Sean Butterworth, Christopher Beach, Muriel Rigout, Kostya S Novoselov, Alexander J Casson, and Stephen G Yeates. 2017. All Inkjet-Printed Graphene-Based Conductive Patterns for Wearable E-textile Applications. *Journal of Materials Chemistry C* 5, 44 (2017), 11640–11648.

[38] Chang-Sei Kim, Stephanie L Ober, M Sean McMurtry, Barry A Finegan, Omer T Inan, Ramakrishna Mukkamala, and Jin-Oh Hahn. 2016. Ballistocardiogram: Mechanism and Potential for Unobtrusive Cardiovascular Health Monitoring. *Scientific Reports* 6, 1 (2016), 1–6.

[39] Hyejung Kim, Sunyoung Kim, Nick Van Helleputte, Torfinn Berset, Di Geng, Inaki Romero, Julien Penders, Chris Van Hoof, and Refet Firat Yazicioglu. 2012. Motion Artifact Removal Using Cascade Adaptive Filtering for Ambulatory ECG Monitoring System. In *2012 IEEE Biomedical Circuits and Systems Conference (BioCAS)*. 160–163.

[40] Jonghwa Kim and Elisabeth André. 2008. Emotion Recognition Based on Physiological Changes in Music Listening. *IEEE Transactions on Pattern Analysis and Machine Intelligence* 30, 12 (2008), 2067–2083.

[41] Kyung Hwan Kim, Seok Won Bang, and Sang Ryong Kim. 2004. Emotion Recognition System Using Short-Term Monitoring of Physiological Signals. *Medical and Biological Engineering and Computing* 42, 3 (2004), 419–427.

[42] Ko Keun Kim, Yong Kyu Lim, and Kwang Suk Park. 2004. The Electrically Noncontacting ECG Measurement on the Toilet Seat Using the Capacitively-Coupled Insulated Electrodes. In *Proc. of the 26th IEEE IEMBS*. 2375–2378.

[43] Paul Kligfield, Leonard S. Gettes, James J. Bailey, Rory Childers, Barbara J. Deal, E. William Hancock, Gerard van Herpen, Jan A. Kors, Peter Macfarlane, David M. Mirvis, Olle Pahlm, Pentti Rautaharju, and Galen S. Wagner. 2007. Recommendations for the Standardization and Interpretation of the Electrocardiogram. Part I: The Electrocardiogram and Its Technology A Scientific Statement From the American Heart Association Electrocardiography and Arrhythmias Committee, Council on Clinical Cardiology; the American College of Cardiology Foundation; and the Heart Rhythm Society for Computerized Electrocardiology. *Journal of the American College of Cardiology* 49, 10 (13 March 2007), 1109–1127.

[44] Jesús Lázaro, Eduardo Gil, Raquel Bailón, Ana Mincholé, and Pablo Laguna. 2013. Deriving Respiration From Photoplethysmographic Pulse Width. *Medical & Biological Engineering & Computing* 51, 1 (2013), 233–242.

[45] Hooseok Lee, Heewon Chung, Jong-Woong Kim, and Jinseok Lee. 2019. Motion Artifact Identification and Removal From Wearable Reflectance Photoplethysmography Using Piezoelectric Transducer. *IEEE Sensors Journal* 19, 10 (2019), 3861–3870.

[46] Gang Li and Wan-Young Chung. 2013. Detection of Driver Drowsiness Using Wavelet Analysis of Heart Rate Variability and a Support Vector Machine Classifier. *Sensors* 13, 12 (2013), 16494–16511.

[47] Suyi Li and Jun Lin. 2009. The Optimal De-noising Algorithm for ECG Using Stationary Wavelet Transform. In *World Congress on Computer Science and Information Engineering*, Vol. 6. 469–473.

[48] Xiaoling Li, Bin Liu, Yang Liu, Jiawei Li, Jiarui Lai, and Ziming Zheng. 2019. A Novel Signal Separation and De-noising Technique for Doppler Radar Vital Signal Detection. *Sensors* 19, 21 (2019), 4751.

[49] J. Lilienthal and W. Dargie. 2019. Extraction of Motion Artifacts From the Measurements of a Wireless Electrocardiogram Using Tensor Decomposition. In *Proc. of the 22nd International Conference on Information*. 1–8.

[50] Yong Gyu Lim, Ko Keun Kim, and Suk Park. 2006. ECG Measurement on a Chair Without Conductive Contact. *IEEE Transactions on Biomedical Engineering* 53, 5 (2006), 956–959.

[51] Wan-Hua Lin, Dan Wu, Chunyue Li, Heye Zhang, and Yuan-Ting Zhang. 2014. Comparison of Heart Rate Variability From PPG With That From ECG. In *The International Conference on Health Informatics*. 213–215.

[52] Guohua Lu, F Yang, JA Taylor, and JF Stein. 2009. A Comparison of Photoplethysmography and ECG Recording to Analyse Heart Rate Variability in Healthy Subjects. *Journal of Medical Engineering & Technology* 33, 8 (2009), 634–641.

[53] Tan Cheng Lu, Peng Liu, Xiang Gao, and Qi Yong Lu. 2014. A Portable ECG Monitor With Low Power Consumption and Small Size Based on AD8232 Chip. In *Applied Mechanics and Materials*, Vol. 513. 2884–2887.

[54] João PV Madeiro, Paulo C Cortez, João AL Marques, Carlos RV Seisdedos, and Carlos RMR Sobrinho. 2012. An Innovative Approach of QRS Segmentation Based on First-Derivative, Hilbert and Wavelet Transforms. *Medical Engineering & Physics* 34, 9 (2012), 1236–1246.

[55] Lerato Mahloko and Funmi Adebesin. 2020. A Systematic Literature Review of the Factors that Influence the Accuracy of Consumer Wearable Health Device Data. *Responsible Design, Implementation and Use of Information and Communication Technology* 12067 (2020), 96.

[56] Alba Martín-Yebra, Federica Landreani, Claudia Casellato, Esteban Pavan, Carlo Frigo, Pierre-François Migeotte, and Enrico G Caiani. 2015. Studying Heart Rate Variability From Ballistocardiography Acquired by Force Platform: Comparison With Conventional ECG. In *2015 Computing in Cardiology Conference (CinC)*. 929–932.

[57] P. F. Migeotte, V. Mucci, Q Delière, L. Lejeune, and Pvd Borne. 2016. Multi-Dimensional Kineticardiography a New Approach for Wearable Cardiac Monitoring Through Body Acceleration Recordings. In *XIV Mediterranean Conference on Medical and Biological Engineering and Computing*. 1125–1130.

[58] Shuto Nagai, Daisuke Anzai, and Jianqing Wang. 2017. Motion Artefact Removals for Wearable ECG Using Stationary Wavelet Transform. *Healthcare Technology Letters* 4 (2017), 138–141.

[59] Jaeyeon Park, Hyeon Cho, Rajesh Krishna Balan, and JeongGil Ko. 2020. HeartQuake: Accurate Low-Cost Non-Invasive ECG Monitoring Using Bed-Mounted Geophones. *Proc. of ACM IMWUT 2020* 4, 3, Article 93 (Sept. 2020), 28 pages.

[60] Konstantinos N. Plataniotis, Dimitrios Hatzinakos, and Jimmy K. M. Lee. 2006. ECG Biometric Recognition Without Fiducial Detection. In *2006 Biometrics Symposium: Special Session on Research at the Biometric Consortium Conference*. 1–6.

[61] Taina Pola and Jukka Vanhala. 2007. Textile Electrodes in ECG Measurement. In *Proc. of the 3rd IEEE ISSNIP*. 635–639.

[62] Merja M Puurtinen, Satu M Komulainen, Pasi K Kauppinen, Jaakko AV Malmivuo, and Jari AK Hyttinen. 2006. Measurement of Noise and Impedance of Dry and Wet Textile Electrodes, and Textile Electrodes With Hydrogel. In *Proc. of IEEE IEMBS 2006*. 6012–6015.

[63] Michael Reardon and Marek Malik. 1996. Changes in Heart Rate Variability With Age. *Pacing and Clinical Electrophysiology* 19, 11 (1996), 1863–1866.

[64] Georgios Rigas, Christos D Katsis, George Ganiatsas, and Dimitrios I Fotiadis. 2007. A User Independent, Biosignal Based, Emotion Recognition Method. In *International Conference on User Modeling*. 314–318.

[65] Anna Rosiek and Krzysztof Leksowski. 2016. The Risk Factors and Prevention of Cardiovascular Disease: The Importance of Electrocardiogram in the Diagnosis and Treatment of Acute Coronary Syndrome. *Therapeutics and Clinical Risk Management* 12 (2016), 1223–1229.

[66] Pritam Sarkar and Ali Etemad. 2020. Self-Supervised ECG Representation Learning for Emotion Recognition. *IEEE Transactions on Affective Computing* (2020).

[67] Suzanne C Segerstrom and Lise Solberg Nes. 2007. Heart Rate Variability Reflects Self-Regulatory Strength, Effort, and Fatigue. *Psychological science* 18, 3 (2007), 275–281.

[68] Matthias Seuter, Alexandra Pollock, Gernot Bauer, and Christian Kray. 2020. Recognizing Running Movement Changes with Quaternions on a Sports Watch. *Proc. of the ACM on Interactive, Mobile, Wearable and Ubiquitous Technologies* 4, 4 (dec 2020), 18.

[69] Yanting Shen. 2020. *ECG Classification and The" Heart Age" Prediction Using Machine Learning*. Ph.D. Dissertation. University of Oxford.

[70] Lin Shu, Yang Yu, Wenzhuo Chen, Haoqiang Hua, Qin Li, Jianxiu Jin, and Xiangmin Xu. 2020. Wearable Emotion Recognition Using Heart Rate Data From a Smart Bracelet. *Sensors* 20, 3 (2020), 718.

[71] Gulbadan Sikander and Shahzad Anwar. 2018. Driver Fatigue Detection Systems: A Review. *IEEE Transactions on Intelligent Transportation Systems* 20, 6 (2018), 2339–2352.

[72] Ernst Simonson. 1953. Gradual Changes of ECG Waveform During and After Exercise in Normal Subjectseffect of Moderate Exercise on the Electrocardiogram in Healthy Young and Middle-Aged Men. *Journal of Applied Physiology* 5, 10 (1953), 584–588.

[73] ML Simoons and PG Hugenholtz. 1975. Gradual Changes of ECG Waveform During and After Exercise in Normal Subjects. *Circulation* 52, 4 (1975), 570–577.

[74] Sunto. 2022. How to Get More Accurate Wrist Heart Rate Readings. https://www.suunto.com/Content-pages/what-should-you-know-about-wrist-heart-rate2/

[75] Motonao Tanaka, Tsuguya Sakamoto, Shigeo Sugawara, Hiroyuki Nakajima, Takeyoshi Kameyama, Yoshiaki Katahira, Shigeo Ohtsuki, and Hiroshi Kanai. 2010. Spiral Systolic Blood Flow in the Ascending Aorta and Aortic Arch Analyzed by Echo-Dynamography. *Journal of Cardiology* 56, 1 (2010), 97–110.

[76] Manal M Tantawi, Kenneth Revett, Abdel-Badeeh Salem, and Mohamed F Tolba. 2015. A Wavelet Feature Extraction Method for Electrocardiogram (ECG)-Based Biometric Recognition. *Signal, Image and Video Processing* 9, 6 (2015), 1271–1280.

[77] Xin Tian, Qiang Zhu, Yuenan Li, and Min Wu. 2020. Cross-Domain Joint Dictionary Learning for ECG Reconstruction From PPG. In *Proc. IEEE ICASSP'20*. 936–940.

[78] G Vega-Martinez, FJ Ramos-Becerril, D Mirabent-Amor, JG Franco-Sánchez, A Vera-Hernández, C Alvarado-Serrano, and L Leija-Salas. 2018. Analysis of Heart Rate Variability and Its Application in Sports Medicine: A Review. *2018 Global Medical Engineering Physics Exchanges/Pan American Health Care Exchanges (GMEPE/PAHCE)* (2018), 1–5.

[79] C Venkatesan, P Karthigaikumar, and S Satheeskumaran. 2018. Mobile Cloud Computing for ECG Telemonitoring and Real-Time Coronary Heart Disease Risk Detection. *Biomedical Signal Processing and Control* 44 (2018), 138–145.

[80] Adriana N Vest, Giulia Da Poian, Qiao Li, Chengyu Liu, Shamim Nemati, Amit J Shah, and Gari D Clifford. 2018. An Open Source Benchmarked Toolbox for Cardiovascular Waveform and Interval Analysis. *Physiological Measurement* 39, 10 (2018), 105004.

[81] Wanhui Wen, Guangyuan Liu, Nanpu Cheng, Jie Wei, Pengchao Shangguan, and Wenjin Huang. 2014. Emotion Recognition Based on Multi-Variant Correlation of Physiological Signals. *IEEE Transactions on Affective Computing* 5, 2 (2014), 126–140.

[82] Xin Wen, Yanqi Huang, Xiaomei Wu, and Biyong Zhang. 2019. A Feasible Feature Extraction Method for Atrial Fibrillation Detection From BCG. *IEEE Journal of Biomedical and Health Informatics* 24, 4 (2019), 1093–1103.

[83] Withings. 2022. Wearing My Watch. https://support.withings.com/hc/zh-cn/articles/360017770597-ScanWatch-Wearing-my-watch

[84] Yadong Xie, Fan Li, Yue Wu, Song Yang, and Yu Wang. 2019. D3-Guard: Acoustic-Based Drowsy Driving Detection Using Smartphones. In *IEEE INFOCOM 2019 - IEEE Conference on Computer Communications*. 1225–1233.

[85] Kohei Yamamoto, Ryosuke Hiromatsu, and Tomoaki Ohtsuki. 2020. ECG Signal Reconstruction via Doppler Sensor by Hybrid Deep Learning Model With CNN and LSTM. *IEEE Access* 8 (2020), 130551–130560.

[86] Han Zhang, Ian Goodfellow, Dimitris Metaxas, and Augustus Odena. 2019. Self-Attention Generative Adversarial Networks. In *International Conference on Machine Learning*. PMLR, 7354–7363.

[87] Mingmin Zhao, Fadel Adib, and Dina Katabi. 2016. Emotion Recognition Using Wireless Signals. In *Proc. of the 22nd ACM MobiCom*. 95–108.

[88] Qibin Zhao and Liqing Zhang. 2005. ECG Feature Extraction and Classification Using Wavelet Transform and Support Vector Machines. In *Proc. of the IEEE ICNNB 2005*, Vol. 2. 1089–1092.

[89] Qiang Zhu, Xin Tian, Chau-Wai Wong, and Min Wu. 2019. ECG Reconstruction via PPG: A Pilot Study. In *Proc. of IEEE BHI 2019*. IEEE, 1–4.